NTNU

Norwegian University of
Science and Technology

The Burridge-Knopoff-Pad Model

A New Model for Studying Noise Generation
& Brake Dynamics

Herman Nylund Ferre

Master of Science in Engineering and ICT
Submission date: February 2018
Supervisor: Bjørn Haugen, MTP
Co-supervisor: Astrid de Wijn, MTP

Norwegian University of Science and Technology
Department of Mechanical and Industrial Engineering

The Burridge-Knopoff–Pad Model: A New Model for Studying Noise Generation & Brake Dynamics

Herman Nylund Ferre

February 2018

MASTER'S THESIS

Department of Mechanical and Industrial Engineering

Norwegian University of Science and Technology

Supervisors:

Associate Professor Bjørn Haugen

Associate Professor Astrid S. de Wijn

Preface

This is a Master's Thesis in Product Development and Materials as part of the study program Engineering and ICT (MTING) at the Norwegian University of Science and Technology (NTNU). The project was carried out during the winter of 2017/2018, at the Department of Mechanical and Industrial Engineering.

This Thesis, studying friction in an enhanced spring–block model, deals with topics under mechanical engineering, specifically tribology, and is suited for anyone with some experience in engineering and physics.

Trondheim, 2018-02-12

Herman N. Ferre

Acknowledgment

I would like express my deepest gratitude and appreciation to my supervisors, Astrid de Wijn and Bjørn Haugen for great scientific and moral support during the execution of this Project.

Additionally, I would like to thank my parents, Grethe Nylund and Preben Ferre, for their love and support during these last couple of months.

H.F.

Summary and Conclusions

In this Thesis, I have presented a new model, which, to the best of my knowledge, has never been studied before. The Burridge-Knopoff–Pad model combines the plain Burridge-Knopoff model with a resonating mass. The model was developed, implemented and analyzed. Findings show that, while more study is needed, results differ. Thus, a first few steps have been taken in order to fully understand the features of the model. While the model in this Thesis is applied in the context of brake squeal, it can be applied to any structure involving friction and structural vibrations.

Sammendrag og konklusjoner

I denne masteroppgaven har jeg presentert en ny modell, som så vidt jeg vet aldri har vært studert tidligere. Burridge-Knopoff–Pad-modellen kombinerer den ordinære Burridge-Knopoff-modellen med en resonerende masse. Modellen ble utviklet, implementert og analysert. Funn viser at, selv om nærmere undersøkelser er nødvendig, er resultatene forskjellige. Dermed har de første skritt blitt tatt for å fullt ut forstå modellens egenskaper. Modellen er i denne oppgaven brukt i sammenheng med bremsehyl, men kan benyttes på andre modeller som involverer friksjon og strukturell vibrasjon.

Contents

Chapter 1

Introduction

1.1 Background

The Burridge-Knopoff model is a model developed in the 1960s as an approach to study friction occurring in the interface between two moving surfaces, more specifically, in the field of seismology for the study of earthquakes, where the two surfaces represent tectonic plates. The model consists of a number of blocks, representing the interface, connected to one of the surfaces and to the adjacent block with springs, while being pulled by the friction from the other surface. It was found that the slipping events resulting from the model exhibit a power law scaling region, consistent with findings that gave rise to the Gutenberg-Richter law.

Brake squeal has been a heavily studied phenomenon for decades. The automotive industry is interested in minimizing the occurrence of squeal which impacts the comfort of vehicle occupants. Brake squeal is thought to result from vibrations due to instabilities in the brake system. Several papers have, as an introductory approach, utilized the Burridge-Knopoff model to describe the interface between the brake disc and pad. In addition to other analyses such as a complex eigenvalue analysis (CEA), the dynamics of several different model configurations—from a one degree-of-freedom model to multi-dimensional models—have been studied in the time domain.

This Thesis describes the analysis of a new model, which, to the best of my knowledge, has never been studied before. The one degree-of-freedom and Burridge-Knopoff models each contain elements we don't know *if* interact with each other in a real-life environment—or *how*. Therefore, this new one-dimensional model combines the Burridge-Knopoff model with the one degree-of-freedom model, resulting in a system with a number of blocks connected to each other as well as to a resonating *pad* connected to a stationary surface with a spring and a damper. It will be referred to as the **Burridge-Knopoff–Pad Model**.

1.2 Objectives

The main objectives of this Thesis are to

1. implement and simulate the new combined Burridge-Knopoff–Pad model, and,
2. investigate the results to see if this brings anything new into the study of brake squeal or friction-induced vibrations.

1.3 Limitations

It is important to note that as this model has never been studied before, things are kept simple in order to explore the basic characteristics. The model is one-dimensional, uniform in masses and spring constants, and the parameters are scaled. In addition, the applied friction law is idealized. The only irregularity introduced to the model in this Thesis is the random displacement of the different blocks.

The study of this model has also been limited by computational power. In order to be able to plot the same results several times, the data is written to files which take time to read, process and plot.

1.4 Approach

As described in Section 3.4, I will implement and simulate the new model for a range of disc speeds. I will then process the results and conduct investigations into features of interest in the

results.

Molecular Dynamics simulations will be carried out using a 2^{nd} order Runge-Kutta scheme, for a range of brake disc speeds. Areas of interest will be identified and investigated. The results will be subjected to post-processing, such as Fourier spectrum analyses, and amplitude and mean value extraction.

1.5 Structure of the Report

In this Thesis, I will first go through the background on the subject in Chapter 2, giving an overview of the theory and what has been studied before. Then I will describe my approach and choice of model in Chapter 3. Results will be shown and discussed in Chapter 4 with summary and conclusions given in Chapter 5.

Chapter 2

Background and Literature

In this chapter, I will explain the principles of the Burridge-Knopoff model, and conduct a study of literature relating to its application in models of earthquake faults. Later, I will explain the principle of disc brakes and go through literature on the study of brake squeal, giving an overview of different models and theories that have been used.

2.1 The Burridge-Knopoff Model

The Burridge-Knopoff model (Burridge and Knopoff, 1967) is a model developed for the study of friction. It is a one-dimensional approach for describing the interactions between a pair of surfaces in contact, sliding along one another (i.e., non-zero relative speed), and describes the interface between the two as a series of blocks connected to the adjacent one(s) through springs (*neighboring springs*). These blocks are also each connected to one surface (the upper surface in the case of Figure 2.1) with another spring (the *pulling spring*).

The governing equation of the model is defined as,

$$m\ddot{X}_j = k_c(X_{j-1} - 2X_j + X_{j+1}) - k_p X_j - F(v + \dot{X}_j) \quad , \tag{2.1}$$

where X_j denotes the position of block j with respect to its equilibrium position. The subscripts c and p stand for "coupling" and "pulling," of which the former is the papers' term for the neighboring spring.

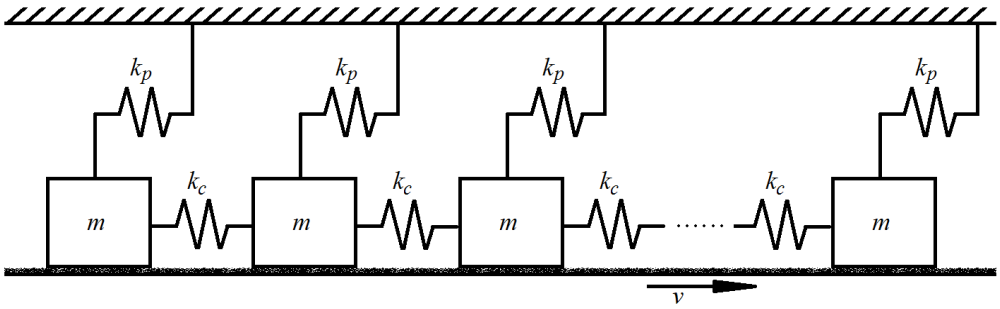

Figure 2.1: Simple graphic of the Burridge-Knopoff model

The rough surface (referred to as *substrate*) causes friction which is governed by the viscous term. Some velocity-weakening friction function is chosen. As the substrate, moving with velocity v, drags the blocks along with it, the force from a pulling spring will eventually exceed the maximum static friction force F_0, leading to a slipping event. This maximum distance is given as $D_0 = F_0/k_p$. As the energy dissipates through friction, the blocks will again come to rest (i.e., become stuck). This is referred to as *stick–slip behavior*.

In the context of brake squeal, the two surfaces represent the two parts of a braking system where one is pressed against the other in order to slow down a vehicle, using friction to transform kinetic energy into heat. Under different circumstances when braking, noises of different frequencies can be heard, and the Burridge-Knopoff model has been used in attempts to study these noises.

2.2 Using the Burridge-Knopoff Model for Earthquake Events

In the seismological field, the Burridge-Knopoff model can be applied to the studies of earthquakes in that its two surfaces are analogous to tectonic plates. The model is therefore an approximation of a fault at which a plate moves laterally (along the fault) with respect to the other.

The version of the Burridge-Knopoff model researched in Carlson and Langer (1989) consists of a completely uniform system with no spatial variations or externally determined stochastic elements. They assume an idealized velocity-weakening friction law. They convert the equation of motion into dimensionless variables, yielding

$$\ddot{U}_j = l^2(U_{j-1} - 2U_j + U_{j+1}) - U_j - \phi(2\alpha v + 2\alpha\dot{U}_j) \quad , \tag{2.2}$$

where $l^2 = k_c/k_p$, and $2\alpha = \omega_p D_0/v_1$. $v = v/(\omega_p D_0)$ is the dimensionless velocity of the substrate (the ratio of the slipping time ω_p^{-1} to the loading time D_0/v), and it shall here be mentioned that the substrate velocity is given in the opposite direction, which can easily be confirmed by knowing that the variable of the friction function is the relative speed between a block and the substrate. v_1 is a characteristic velocity for which the friction is half the maximum static friction force, and $U = X/D_0$ is a block's position normalized by its maximum distance before slipping.

The friction law chosen by Carlson and Langer (1989) is given (in its dimensionless form) by

$$\phi(y) = \frac{1}{1+|y|}\mathrm{sgn}(y) \quad , \tag{2.3}$$

and $\phi(0)$ (zero velocity, i.e., stuck state) is any value within ± 1, whatever force is required to counteract that of the springs (up to ± 1, at which point the block will slip).

The paper first looks at a trivial solution

$$U = -\phi(2\alpha v) = \text{const.} \quad , \tag{2.4}$$

where there are no springs, and the position is given by the friction force. The paper shows that such a friction law makes the solution unstable against small perturbations of all wavelengths. It is shown that this instability does not cause divergence, but rather that small deformations will be amplified during slipping. This friction law is changed in a subsequent paper (Carlson et al., 1991) which I will discuss later. Further, the article discusses periodic behavior when using only the pulling springs and the friction force,

$$\ddot{U} = -U - \phi(2\alpha v + 2\alpha \dot{U}) \quad , \tag{2.5}$$

and describes a simulation with almost exactly uniform spacing, where the small irregularities are amplified during the slipping event by the same mechanism as previously mentioned, leaving the system in an even more irregular state after all the blocks are stuck. A large α yields a small ϕ, giving $\ddot{U} \approx -U$. One cycle consists of a loading period $\tau_L = 2/v$, and a slipping period τ_S which is of order π due to the choice of units so that $U \cong \cos(\tau)$.

The paper shows how the slipping events involve smaller, connected groups of blocks, as opposed to motions concerning the entire system. It categorizes events into three categories, "microscopic," "localized," and "delocalized," depending on how many blocks are involved in a particular event. They analytically identify certain solutions involving a group of blocks slipping together, and discuss how a pulse in a slipping zone won't exceed the limits of the zone unless the zone is very large, i.e., stay localized. For very large zones, where many blocks are in positions where their spring forces are close to overcoming the maximum static friction force, a pulse may become delocalized and propagate out of the zone.

Further, they conduct numerical simulations with parameters $v = 0.01$, $l = 10$, $\alpha = 2.5$, and $N = 50$, and provide plots from two different time spans. One of them shows a relatively quiet period with two small events involving the same group of eight blocks. Additionally, we see minor periodic one-block events. It should be noted that these events all have velocities less than the pulling speed. Another time span shows a greater event defined as "localized," where blocks are slipping at higher velocities than the pulling speed v, although smaller than unity, which is the maximum slipping velocity. A third plot shows a great event which only happens about one time per loading period. Here, the event spreads out to system edges and is reflected back, and eventually dies.

Relation to the Gutenberg-Richter Law

By defining the moment as

$$M = \sum_j \delta U_j \tag{2.6}$$

and the corresponding magnitude as $\mu = \ln M$, let $\mathscr{R}(\mu)$ be the frequency of events with a magnitude $\geq \mu$ (for a small $\mathrm{d}\mu$, $\mathscr{R}(\mu)\mathrm{d}\mu$ is the frequency of events with magnitudes between μ and $\mu + \mathrm{d}\mu$). The paper cites Gutenberg and Richter in that the function has the form

$$\mathscr{R}(\mu) = \frac{A}{M^b} = Ae^{-b\mu} \quad . \tag{2.7}$$

A is an unknown independent constant, and $b \cong 1$ is determined empirically from observations around the world. Plotting the logarithm of this function,

$$\ln(\mathscr{R}(\mu)) = \ln(A) - b\mu \quad , \tag{2.8}$$

against the magnitude, μ, they show that for very small magnitudes, there are irregular variations with several peaks in the frequency. However, for increasing magnitudes, the graphs are linear with a slope of $-b$. When $\alpha \geq 2.5$, b is approximately equal to unity, which agrees with the Gutenberg-Richter law. This portion of the distribution is called the "scaling region." One plot shows the distribution for $\alpha = 1$ (friction is increased), and the slope of this scaling region is much flatter than unity, telling us that larger-magnitude events occur more frequently. For the largest magnitudes of the distribution, events occur more frequently than would fit the scaling region; however, to a lesser extent for $\alpha = 1$. For a total fault length L and (in our units) a maximum displacement of a block $\delta U = 2$, the maximum moment is $2L$, giving a magnitude $\mu_L = \ln(2L)$, which is shown to be an upper bound for the magnitude.

The distribution of events in the scaling region is found to be independent of the system size L given that v is sufficiently small. For short faults, the analysis predicts that great (delocalized) earthquakes recur almost periodically.

The paper highlights certain limitations and missing properties of the model, naming its one-dimensionality as the most serious one. Although great earthquakes involve movement in one dimension, the paper states that there are small slips occurring in the two-dimensional interface between the plates. The strain fields extend into the plates also outside of the interface, and this is not handled by the one-dimensional block–spring configuration. Also, it seems likely that the two-dimensional nature of the localized slipping events would affect the scaling distribution. Therefore, an important unanswered question in the paper is how to make the model more realistic.

Further, the lack of interaction between different faults, or distant areas of the same fault, is discussed. The idealized friction law chosen in the paper probably eliminates the risk of aftershocks, in that there is no possibility of communication between two separate slipping zones, if there is at least one stuck block in between.

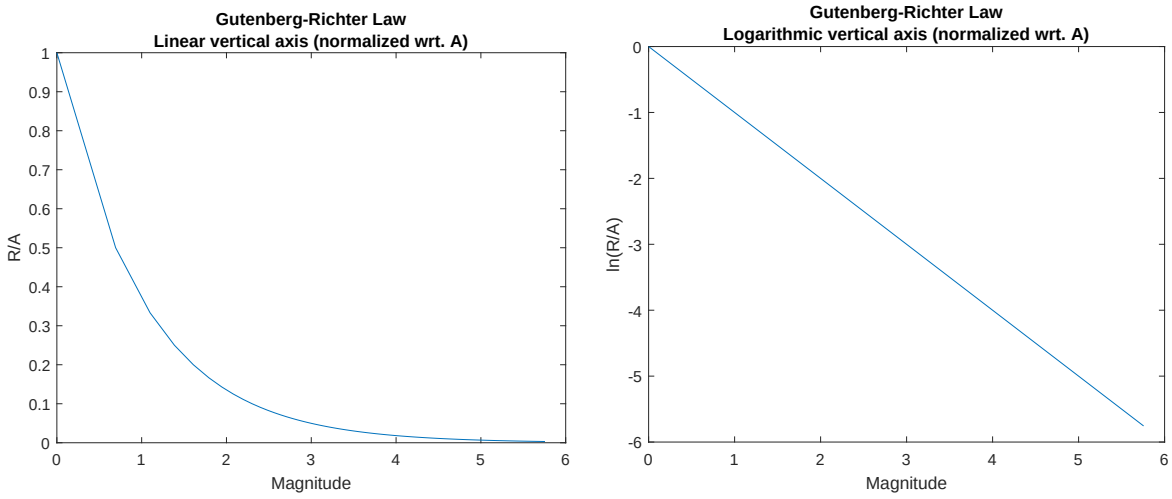

(a) Linear vertical axis (Eq. 2.7)

(b) Logarithmic vertical axis (Eq. 2.8)

Figure 2.2: The Gutenberg-Richter law, $b = 1$. Note that $\mathscr{R}$ is scaled by the unknown parameter A.

Further Studies

Carlson et al. (1991) decide to go further in studying the transition between localized and greater delocalized events. As previously mentioned, they redefine their friction law in to one where no backwards motion is allowed, and another variable σ is introduced:

$$\phi(y) = \begin{cases} (-\infty, 1] & y = 0 \\ \dfrac{1-\sigma}{1+\frac{y}{1-\sigma}} & y > 0 \end{cases} . \tag{2.9}$$

Similarly to Eq. 2.3, for zero velocity the friction force will be whatever is required to keep a block stuck—with its new interval $(-\infty, 1]$, however, it is clear that no negative velocity is permitted. In addition, while the maximum static friction force remains unity, the maximum sliding friction force (i.e., for a y infinitesimally greater than 0) is $1-\sigma$.

The paper argues that this new friction law will cause slipping events that start abruptly with acceleration proportional to σ rather than the third derivative proportional to the substrate velocity v, consequently making the individual events independent of v. They discuss how the computational procedure has been simplified, in that they are now able to solve the system with the substrate stationary ($v = 0$), letting all the blocks come to rest, and then find the position and

time of the next slipping event by locating the block with the greatest spring forces.

It was earlier argued that the instability from the velocity-weakening friction law amplified the irregularities during a slipping event (Carlson and Langer, 1989), and it is stated that this is true for irregularities of a smaller length scale than that of the event; and irregularities of a bigger scale are smoothed. A smooth region will slip in a large, delocalized event, creating irregularities which later will be smoothed during a minor, localized event. Thus the paper argues that the model creates both of these two separate classes of events, where the statistical distribution of the smaller events are governed by large ones.

Further, the article aims to define a "crossover" moment $\tilde{\mathbf{M}}$ (located between the lower and upper cutoff, $\mathbf{M_1}$ and $\mathbf{M}^*$ respectively), separating localized and delocalized events, as the scaling region (localized) and the fitted line to the data of the delocalized events have different constants, together constituting a pair of power laws for the frequency distribution $D(\mu)$ given as

$$D(\mu) = \begin{cases} \mathbf{A}(\tilde{\mathbf{M}}/\mathbf{M})^{b} & \mathbf{M_1} < \mathbf{M} < \tilde{\mathbf{M}} \\ \mathbf{A}'(\mathbf{M}/\mathbf{M}^*)^{-b'} & \tilde{\mathbf{M}} < \mathbf{M} < \mathbf{M}^* \\ 0 & \mathbf{M} < \mathbf{M_1} \cup \mathbf{M}^* < \mathbf{M} \end{cases} . \tag{2.10}$$

The paper plots frequency vs magnitude plots for several values of $l = k_c/k_p$ and these results can be used to extrapolate results to situations where $l \sim 100$. It concludes that the model is governed by two dimensionless variables, σ (or v as previously studied) and the friction constant α, however also in addition to the dimensionless stiffness constant l.

2.3 The Study of Brake Squeal

Disc brake squeal has for decades been, and still is, an important topic of study. Different models have been employed in the attempt to investigate the source of this phenomenon as well as to predict it, and the large amount of articles on the matter have been subject to a handful of review articles (e.g., see Cantoni et al., 2009; Coudeyras et al., 2009). Many physical experiments have also been carried out; however, I will not go into great detail on these unless this is important regarding my own model.

A disc brake assembly is characterized by a disc mounted to the axle hub, thereby rotating with the wheel, with pads of a friction material pressed against it when the brake is applied. The caliper, which is mounted in such a way as to hold it stationary, contains hydraulic pistons which press the pads onto the disc, as the hydraulic pressure increases upon application of the brakes. The friction force between the pads and the disc will then slow down the wheel, transforming its kinetic energy into heat. The pad is in itself an assembly, as it contains the friction material, a backing plate, and other components—however, usually it is in its entirety referred to as a *pad* (Kinkaid et al., 2003), as will also be the case in this Thesis. The disc is usually made of gray iron, and modern systems usually have different features to ensure proper cooling; e.g., having the disc be made from two plates with fins in between acting as air ducts, and giving the disc a top hat-like shape in order to increase the distance the heat must travel to reach the wheel bearings.

Rhee et al. (1989) state that noises can be classified into categories; low frequency, and medium-to-high frequency. Low frequency noises are in the range of 100 Hz to 1000 Hz, can be felt by the driver through the pedals or steering wheel, and are probably best described with terms like *judder*, *moan*, or *groan*. On the other end of the scale, the medium-to-high frequencies (1 kHz to 18 kHz) are usually heard as a squeal or squeak. The authors find that the theory of squeal as a result of rapid friction increase does not hold. They find that a brake being dragged generates more noise than one being stopped, and thus they state that there is no correlation between generated noise and increased friction.

One Degree-of-Freedom Model

A one degree-of-freedom model is the simplest way of describing a dry friction oscillator. Galvanetto (1999) shows its characteristics and behavior based on different disc speeds, which give different stick phase durations, or no slip at all when the disc speed is adequately high. Often, the model includes a damper, as in Matsui et al. (1992). However, the one degree-of-freedom model is, according to Cantoni et al. (2009), not suitable to describe brake vibration and noise.

Vibration Mechanisms

Ibrahim (1994) identifies four possible mechanisms of friction-induced disc brake vibration.

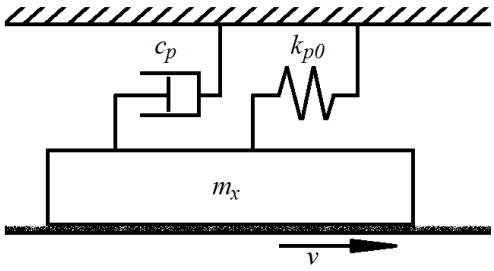

Figure 2.3: One of many ways to illustrate the one degree-of-freedom model with damping.

Stick–Slip. The stick–slip phenomenon describes a situation where a block is stuck to the moving surface due to the friction holding it in place. Given an appropriate range of parameters, such as the disc speed, spring stiffness, etc., the block will be dragged up to a certain displacement at which the spring forces overcome the static friction, causing the block to slip. From there, the block will go back in the opposite direction exhibiting oscillations characterized by the damping of its movement, and eventually its movement will synchronize with the disc (i.e., the block has re-stuck to the disc). Most studies of friction-induced vibration assume that stick–slip behavior occurs because the dynamic friction is lower than the static friction (Ibrahim, 1994). It has also been found that the frequency of the stick–slip motion increases with the disc speed, with its maximum approaching the natural (i.e., undamped) frequency of the system. An expression for the critical disc speed beyond which stick–slip behavior cannot occur has been derived by Brockley et al. (1967).

Sprag–Slip. Spurr (1961) investigated the theory of sprag–slip, in which the pad could be viewed as a rod pivoting around a point, as illustrated in Figure 2.4. The other end of the rod, where it meets the slider, is leading the pivot point with respect to the disc movement axis. Thus, as the friction pushes the rod forward, it becomes wedged between the disc and the pivot point, deforming elastically as the compressive forces increase, until it finally slips and the original condition is restored and the cycle can repeat. Experiments were carried out, where the pad was ground so as to reduce its contact area to a certain portion. It was found that the squeal would only occur when the contact area was within a minimum distance from the leading edge of the pad. The angle of the line drawn through the point where the pad is fixed to its actuator, and the midpoint of the contact area will correspond to the angle of the rod, hanging from the pivot point and touching the disc with the other end. Consequently, there is a characteristic angle

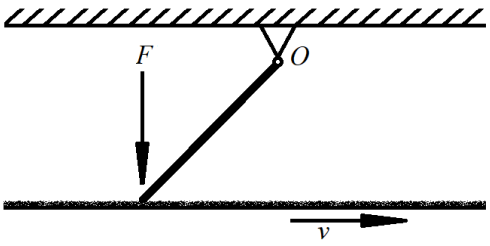

Figure 2.4: Simple illustration of the sprag–slip model. The braking force F pushes the rod onto the rough surface.

defining the transition between the squeal and no-squeal régimes. The author also notes that during squeal, the caliper experienced violent oscillations, provided the squeal contained low-frequency components which the caliper was able to follow. Kinkaid et al. (2003) refers to other authors pointing out that the disc, pad, and caliper are the most significant vibrating elements during squeal.

Velocity-Weakening Friction, whose negative force–velocity slope gives self-excited vibrations. This is easily explained by comparing it with a damper, which has a positive force–velocity slope which gives a higher "resistance" at higher velocities. The friction works the opposite way by dissipating less at higher speeds. This is shown mathematically in the next Subsection, "Instability Condition for Velocity-Weakening Friction."

While this is supported by Kinkaid et al. (2003), who point out that a velocity-weakening friction law as a reason for squeal has become a school of thought, Rhee et al. (1989) refers to authors pointing out that also the assembly's structural instability factors should be considered. However, although they can describe conditions where squeal might occur, the physical phenomenon is not clearly defined. Rhee et al. also highlight the importance of taking temperature into consideration. This will affect the various properties of the rubbing surfaces, as well as the surfaces themselves, and wear rates. Furthermore, the occurrence of brake squeal might also be dependent on how the brakes are applied.

Ostermeyer (2010) also looks at temperature, and writes that an investigation of the tribological interface of the pad reveals friction-intensive surface structures, called "patches." The patches are created permanently from wear and heat, but disappear over time. The continuous appearance and disappearance of these patches form an equilibrium. The patches' vibration frequencies and the local friction power vary as a result of different patch sizes and heights.

He compares these patches to the agglutinations on a piece of sandpaper when sanding wood. While one would think these local and random vibration effects would smooth out, it is stated that they instead are synchronized giving in-phase vibrations of patches of significant size. Ostermeyer agrees that the brake systems have a generally falling friction curve.

Modal Coupling. The changes in friction as a result of modal coupling are necessary for the occurrence of self-excited vibration. Taking both in-plane and out-of-plane vibrations into consideration, Hoffmann et al. (2002) found that the friction force acts as a cross-coupling force between the in-plane and out-of-plane motions.

Instability Condition for Velocity Weakening Friction

A one degree-of-freedom model as shown in Figure 2.3 being dragged by a substrate with speed v_0 in the opposite direction to its displacement from its equilibrium x, with a friction force as a function of the relative velocity given by $F(v_{rel})$, has the following governing equation. Note that in this derivation—for simplicity—any subscripts seen in the Figure are removed, yielding the block mass given by m, the damper coefficient by c, and the spring constant by k.

$$m\ddot{x} = -c\dot{x} - kx - F(\dot{x} + v_0) \quad , \tag{2.11}$$

where $v_{rel} = \dot{x} + v$ has been substituted into the friction function. A velocity-weakening friction law can be expressed as

$$F(v_{rel}) = F_0 - \eta(v_{rel} - v_0) + \mathcal{O}\left((v_{rel} - v_0)^2\right) \quad , \tag{2.12}$$

expanded around the substrate speed v_0, with $F_0 = F(v_0)$.

Furthermore, we look at a very small perturbation ξ of x from its equilibrium position x_0, i.e., $x = x_0 + \xi$. Thus, the velocity and acceleration are given by $\dot{\xi} = \dot{x}$, $\ddot{\xi} = \ddot{x}$, respectively. Such a small perturbation enables us to approximate the friction with the tangent of the friction curve for v_0, of slope $-\eta$. Hence we ignore the higher-order term in Equation 2.12, and insert the linear part

into Equation 2.11, removing any terms that cancel each other out:

$$\begin{aligned} m\ddot{x} &= -c\dot{x} - kx - F(\dot{x} + v_0) \\ &= -c\dot{x} - kx - \Big[F_0 - \eta\big((\dot{x} + v_0) - v_0\big)\Big] \\ &= -c\dot{x} - kx - F_0 + \eta\big((\dot{x} + v_0) - v_0\big) \\ &= -c\dot{x} - kx - F_0 + \eta\dot{x} \quad , \end{aligned}$$

resulting in

$$m\ddot{x} = -(c-\eta)\dot{x} - kx - F_0 \quad . \tag{2.13}$$

Inserting for x, $\dot{x}$, and $\ddot{x}$,

$$m\ddot{\xi} = -(c-\eta)\dot{\xi} - k(x_0 + \xi) - F_0 \quad ,$$

also noting that on a block in equilibrium ($\dot{x} = 0$) pulled with substrate speed v_0, the spring and friction forces are equal and oppositely directed, thus $F_0 = -kx_0$,

$$\begin{aligned} m\ddot{\xi} &= -(c-\eta)\dot{\xi} - k(x_0 + \xi) + kx_0 \\ &= -(c-\eta)\dot{\xi} - k\xi \quad ; \end{aligned}$$

the resulting equation is

$$m\ddot{\xi} + (c-\eta)\dot{\xi} + k\xi = 0 \quad . \tag{2.14}$$

Assuming a solution $\xi = Ce^{\lambda t}$, where C is a constant, we get the characteristic equation with its roots

$$m\lambda^2 + (c-\eta)\lambda + k = 0 \tag{2.15}$$

$$\lambda_{\pm} = -\frac{c-\eta}{2m} \pm \frac{\sqrt{(c-\eta)^2 - 4mk}}{2m} \tag{2.16}$$

$$\lambda_{\pm} = \frac{\eta - c}{2m} \pm i\frac{\sqrt{4mk - (\eta - c)^2}}{2m} \quad . \tag{2.17}$$

The system is unstable if $\mathrm{Re}(\lambda)$ is positive, which will be the case if the friction function slope is steeper than that of the damper ($\eta > c$).

Use of the Burridge-Knopoff Model

Some papers use the Burridge-Knopoff model or variations of it—presumably independently developed, as there are no mentions of or references to Burridge and Knopoff—as a starting point. It's either briefly mentioned as a concept or illustration before carrying out real-system experiments, or used in numerical simulation. Galvanetto (1999) looks into the model, providing conditions for the occurrence of stick and slip phases. Relating the model to real-life elements, Ostermeyer (2010) points out that the patches' change in size and number are irrelevant as they live on a slow time scale relative to the patch vibrations. Through the polymeric matrix, the patches are coupled to each other. Furthermore, the patches are transferring loads to the pad itself. As a result, the patches can be compared to the blocks of the Burridge-Knopoff model. As a consequence of the coupling between the blocks, the global friction force along the pad surface shows significant oscillations as opposed to an unsynchronized, decoupled state.

The Combination of Two Models

A Burridge-Knopoff-like model where the upper surface, to which the blocks are connected, is allowed to move has never been studied before. The original Burridge-Knopoff and one degree-of-freedom models each have elements to them, and we don't know if—or how—these elements might interact with each other in a real-life environment. The Burridge-Knopoff–Pad model is a combination of these to models, and the study of this model forms the basis of this Thesis.

Limitations of Model Study

While a study of mathematical models might give an insight into the dynamics of a the particular system of masses, clearly it does not cover every aspect of a real-life brake system. As Cantoni et al. (2009) point out, almost 80 years of study has provided no major practical results, and in order to create a model as realistic as possible, all the components of a vehicle's suspension system will probably have to be considered.

For instance, any irregularities in the surfaces will impact the friction; however, adding this element to a numerical model accurately is a challenge. Matsui et al. (1992) also note that variation in friction induces an angular moment around the pad's centroid, resulting in varying ef-

fective brake force along the pad in the axis of disc travel. Furthermore, temperature is another variable affecting the friction as well as material properties which is usually not included in such models. Ouyang et al. (2005) suggests that temperature can be handled in a sophisticated friction law.

A recent paper by Denimal et al. (2017) states that the contact interfaces between the different parts of the brake assembly must be taken into consideration in simulations, in addition to the pad–disc interface. In the industry, stability analyses and complex eigenvalue analyses of CAD models are used in the effort to detect and predict squeal. The complex nature of the brake squeal makes it difficult to predict instabilities with a single configuration.

On November 30, 2017, Rowena Crockett of the Swiss Federal Laboratories for Materials Science and Technology (Empa) gave a seminar at the Department of Mechanical and Industrial Engineering at NTNU, "Wear Protection for Kinetic Art." The topic was a study of how one could minimize wear and at the same time maintain noise between two moving parts of a kinetic artwork by Jean Tinguely. The interface of the two parts were studied; however, just as Denimal et al. (2017) point out that instabilities in brake squeal depend on the entire assembly, so do the noise and wear in the artwork.

Chapter 3

Implementation of the Brake Model

3.1 Choice of Model

In this Thesis, I will implement and study a model which, to the best of my knowledge, has never been studied before. The model implemented combines the one-dimensional Burridge-Knopoff model (Burridge and Knopoff, 1967) with the one degree-of-freedom model (e.g., see Matsui et al., 1992; Ibrahim, 1994). Instead of having the blocks connected directly to the upper surface as in the Burridge-Knopoff model, they are connected to a *pad*, which is in turn connected with a spring and a damper to the upper surface (*caliper*). The model is shown in Figure 3.1 and its governing equations are given by

$$\begin{aligned} m_u \ddot{u}_j &= k_c(u_{j-1} - 2u_j + u_{j+1}) - k_p(u_j - x) - m_u \phi(v + \dot{u}_j) \\ m_x \ddot{x} &= -c_p \dot{x} + k_p \sum_j (u_j - x) - k_{p0} x \end{aligned} \quad , \tag{3.1}$$

where ϕ is the friction law given in Equation 3.5, u_j is the position of block j, and x is the position of the pad, relative to their position defined by the situation in which all springs are in equilibrium simultaneously, without any damping or friction forces acting on any part of the model. In other words; with all springs relaxed and all velocity components equal to zero, the positions of the pad and each block are all zero. Hereinafter, this position is for each element referred to as its *zero position*, carefully avoiding the term "equilibrium" as equilibrium is dependent on the total state of the system, and with the introduction of friction, can be the case

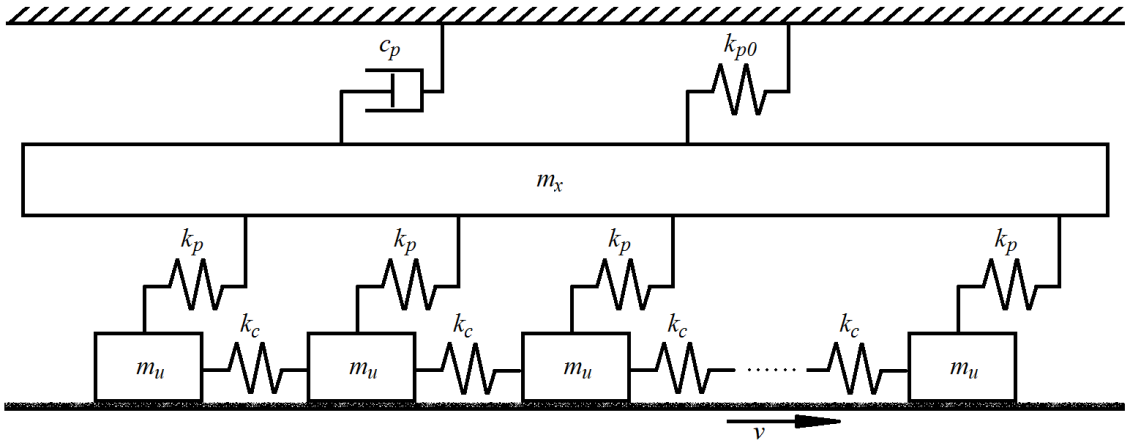

Figure 3.1: Simple graphic of the combined Burridge-Knopoff–pad model. Parameters are given in Table 3.1.

also for non-zero displacements.

Constants and Parameters

Only a subset of all the constants and parameters need to be chosen for the simulation. The following paragraphs will explain the choice of parameters, and a complete overview is provided in Table 3.1—including the values that are used in normal simulations, unless otherwise specified.

The mass of each block, m_u, is proportional to the mass of the pad, m_x divided by the number of blocks, N. Similarly, the spring constant between the pad and a block, k_p, is proportional to the upper spring constant divided by the number of springs (i.e., the number of blocks, N). This is done to ensure that the total force from the disc through the blocks onto the pad is the same irrespective of the number of blocks.

The neighboring spring stiffness is proportional to N, in order for the blocks as a whole to have the same axial stiffness as they would if they were one single element. This is proven by looking at the stiffness of any element, which is given by $k = \frac{EA}{L}$. The length of one block, $L = \frac{L_{tot}}{N}$, is then substituted into the formula, giving $k = \left(\frac{EA}{L_{tot}}\right)N$.

The damping constant c_p is given by the damping ratio $\zeta = \frac{c_p}{c_{\text{crit}}}$, where the critical damping coefficient is given by $c_{\text{crit}} = 2\sqrt{m_x K}$. Here, K is the constant of the single spring equivalent to the system of springs connected to the pad; $K = k_{p0} + Nk_p$ for a system of N blocks. Since Nk_p is constant due to the proportionality of k_p, the critical damping coefficient remains constant.

Table 3.1: Overview of constants and parameters with values.

	User-specified parameters		
Parameter	Symbol	Value	
Number of blocks	N	100	
Pad mass	m_x	100	
Caliper–pad spring constant	k_{p0}	100	
Damping ratio	ζ	$\frac{1}{12}$	
Maximum static friction force	F_0	1	
Friction law scaling parameter	σ	0.01	(See Equation 3.5)
Disc speed	v	*Varying*	(Specified in plots)
Block mass scaling factor	s_m	1	
Pulling spring constant scaling factor	s_p	1	
Neighboring spring scaling factor	s_c	0.01	

	Derived parameters		
Parameter	Symbol	Value	Given by
Mass of block	m_u	1	$s_m \frac{m_x}{N}$
Pulling spring constant	k_p	1	$s_p \frac{k_{p0}}{N}$
Neighboring spring constant	k_c	100	$s_c k_{p0} N$
Critical damping coefficient	c_{crit}	$2\sqrt{20000} \approx 282.84$	$2\sqrt{(k_{p0} + N k_p) m_x}$
Damping coefficient	c_p	$\frac{1}{6}\sqrt{200000} \approx 23.57$	ζc_{crit}

Choice of Time Step Size

The choice of time step size, δt, was based upon the mode of vibration having the greatest frequency. Based on the spring constants in the model, this mode is described by adjacent blocks vibrating with opposite phases; i.e., when they move toward and from one another. The natural, undamped frequency of this mode is given by

$$\omega = 2\pi f = \sqrt{\frac{2(2k_c) + k_p}{m_u}} \quad . \tag{3.2}$$

The prefactor of 2 appears due to the fact that while the displacement of a block is relative to a fixed position, the compression or extension of the spring is not. Rather, the latter is relative to the adjacent block's displacement. In the case of two blocks moving toward one another, the spring is compressed twice the displacement of a block, because it is compressed from each side. As a consequence of the doubled compression, the force from the spring is also doubled.

With a safety factor of $\frac{1}{20}$ and the relevant parameters taken from Table 3.1, a possible time step size is given by

$$\Delta t = \frac{1}{20f} = \frac{1}{20}\frac{2\pi\sqrt{m_u}}{\sqrt{4k_p + k_c}} = 0.015688 \quad . \tag{3.3}$$

Using this as a guideline and a definite upper bond, in order to promote numerical stability while still considering computational efficiency, the time step size for the model configuration used in this Thesis was chosen to be

$$\Delta t = 0.005 \quad . \tag{3.4}$$

Friction Law

Furthermore, I chose to use a friction law similar to Eq. 2.9, although without blocking backwards movement. The possibility of backwards movement must necessarily be allowed in this simulation, as this is a necessary feature due to the fact that the blocks are pulled backwards by the disc up to a point where the pulling spring overpowers the friction force, sending the block

in the opposite direction. The friction law is given by

$$\phi(y) = \begin{cases} F_0[-1,1] & y = 0 \\ F_0 \dfrac{1-\sigma}{1+\frac{|y|}{1-\sigma}} \operatorname{sgn}(y) & y \neq 0 \end{cases}, \tag{3.5}$$

shown in Figure 3.2. The input value y is any the relative velocity of two bodies in contact, and σ is a scaling parameter used for adjusting the slope of the friction law and the maximum kinetic friction. The friction force acting on a specific block is of course dependent to the normal force acting on it by the disc. This is handled by multiplying the force with the mass of the block, as can be seen in Equation 3.1.

Miscellaneous

A block can re-stick to the disc if the following conditions are met (Xia et al., 2005):

- its velocity is less than a predetermined threshold velocity v_0;
- its velocity is decreasing, i.e., negative acceleration; and
- the spring forces acting on the block are less than the maximum static friction force.

The program is coded in C++ using Microsoft Visual Studio 2015, making use of the Eigen library. All plots are made in MATLAB.

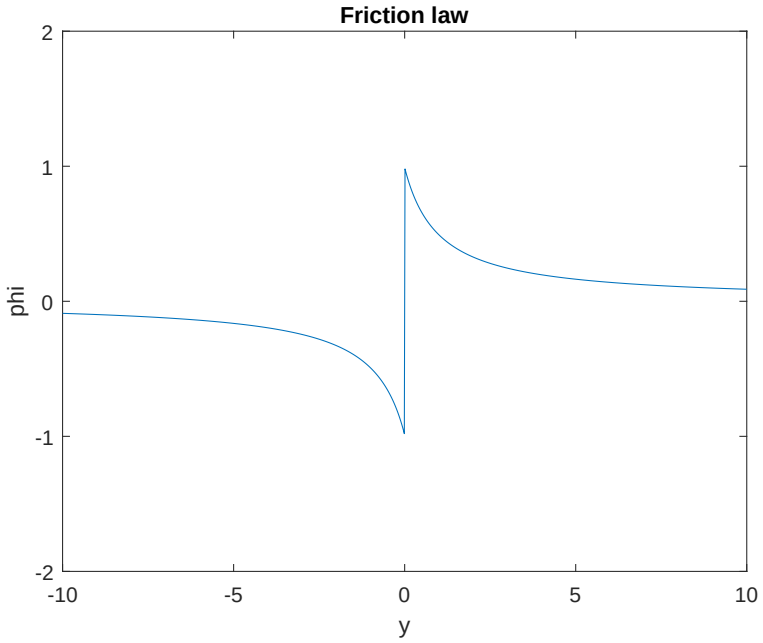

Figure 3.2: Chosen friction law (Equation 3.5): $\sigma = 0.01$, $F_0 = 1$.

3.2 Numerical Scheme

The chosen numerical scheme for the computation is a Runge-Kutta 2$^{\text{nd}}$ order accurate predictor–corrector method known as the *Midpoint Method*, defined for any given function y as

$$\begin{aligned} y^* &= y^n + \frac{\Delta t}{2} f(y^n) \\ y^{n+1} &= y^n + \Delta t f(y^*) \end{aligned} \quad , \tag{3.6}$$

where $f(y) = \frac{d}{dt}(y)$ and the superscripts denote the time step. The predictor step is executed on both the blocks and the pad before the corrector step concludes the process.

The 2$^{\text{nd}}$ order ODEs are solved for every block j and the pad using a vector:

$$\vec{y} = \begin{bmatrix} y \\ \dot{y} \end{bmatrix} \qquad \dot{\vec{y}} = f(\vec{y}) = \begin{bmatrix} \dot{y} \\ \ddot{y} \end{bmatrix} \quad , \tag{3.7}$$

where substituting 3.1 for $\ddot{y}$, gives

$$\vec{u}_j = \begin{bmatrix} u_j \\ \dot{u}_j \end{bmatrix} \qquad \dot{\vec{u}}_j = \begin{bmatrix} \dot{u}_j \\ \frac{1}{m_u}\Big[k_c(u_{j-1} - 2u_j + u_{j+1}) - k_p(u_j - x) - m_u\phi(v + \dot{u}_j)\Big] \end{bmatrix}$$
$$\vec{x} = \begin{bmatrix} x \\ \dot{x} \end{bmatrix} \qquad \dot{\vec{x}} = \begin{bmatrix} \dot{x} \\ \frac{1}{m_x}\Big[-c_p\dot{x} + k_p\sum_j(u_j - x) - k_{p0}x\Big] \end{bmatrix} . \tag{3.8}$$

3.3 Debugging

In order to verify that the program is obeying physical laws and yielding reliable results, tests were performed during development. The model consists of different types of springs as well as a damper, and the chosen procedure was to split it into three parts that were tested separately. The first two tests pertain to the governing equation of the blocks, and the third test pertains to that of the pad. This is done by deactivating certain features such as friction or springs, or hold parts of the model stationary to reduce the amount of degrees of freedom. From there, the results can be compared to known solutions.

Governing Equation of the Blocks

The first test was conducted by removing the friction and the neighboring springs, and holding the pad stationary. This cancels out all terms in the equation except the one related to the pulling spring. Thus, when solving the equation, now reduced to the type $F = -kx$, releasing the block(s) from any non-zero initial displacement, one should expect to see harmonic oscillations. See Figure 3.3.

However, it is more importantly also proven quantitatively by verifying that the total system energy is conserved:

$$\sum E = E_{\text{kin}} + E_{\text{pot}} = \text{const.}, \tag{3.9}$$

which is done for the first test with only the pulling springs, and the second test with only the

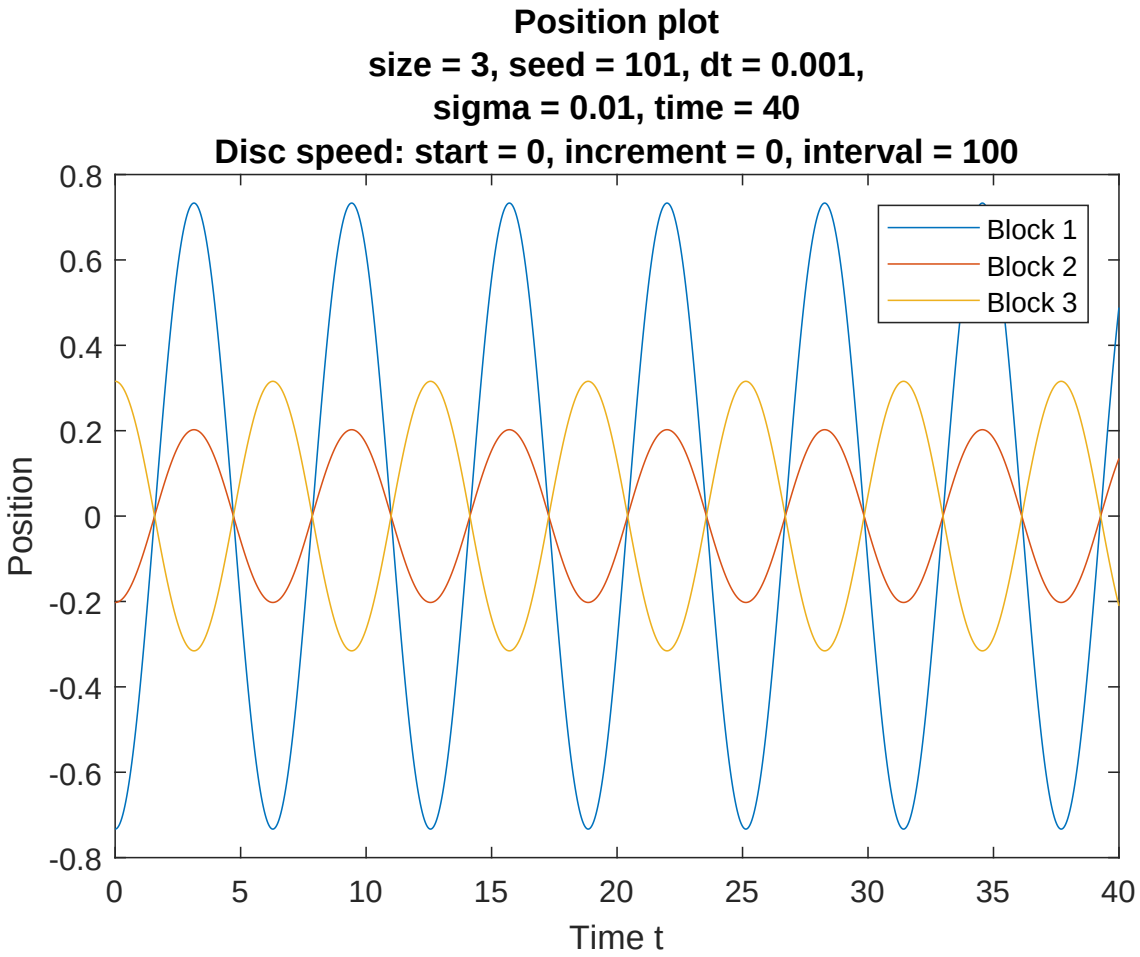

Figure 3.3: Position plot showing the position of three independent blocks only connected to the stationary pad by a pulling spring each, as a function of time. Harmonic oscillations for each block can easily be visually determined.

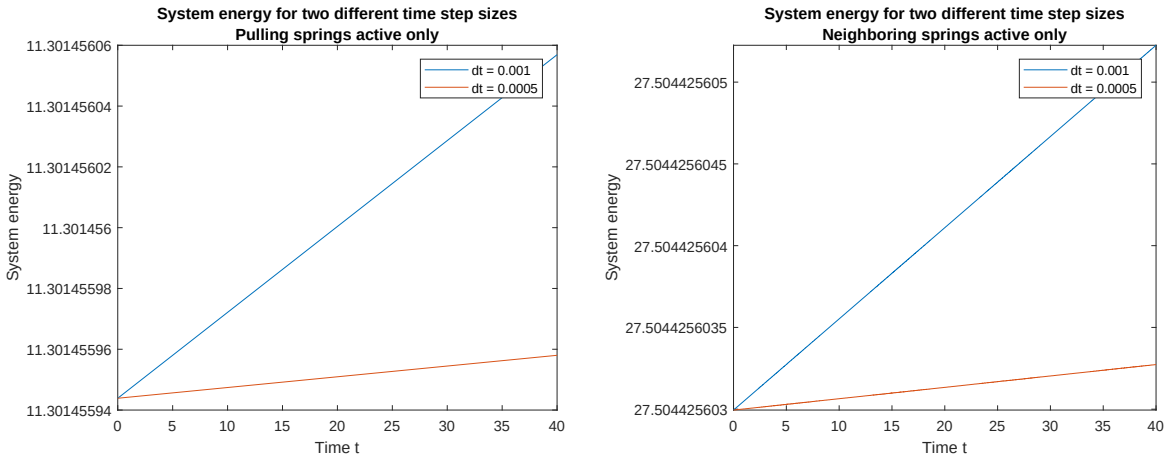

(a) Pulling springs

(b) Neighboring springs

Figure 3.4: System energy for two different time steps, with only pulling springs (left) and only neighboring springs (right).

neighboring springs. The sums of system energy for test 1 and 2, respectively, are given as

$$\begin{aligned} \sum E_{test1} &= \frac{1}{2} m_u \sum_{j=1}^{N} \dot{u}_j^2 + \frac{1}{2} k_p \sum_{j=1}^{N} u_j^2 \\ \sum E_{test2} &= \frac{1}{2} m_u \sum_{j=1}^{N} \dot{u}_j^2 + \frac{1}{2} k_c \sum_{j=2}^{N} (u_j - u_{j-1})^2 \end{aligned} \quad . \tag{3.10}$$

The left and right hand graphs in Figure 3.4 show the system energy over time for the pulling and neighboring springs, respectively, from simulations using two time step sizes, $\Delta t = 0.001$ (as used in Xia et al. (2005)) and half of that ($\Delta t = 0.0005$). As t increases, we see that the system energy accumulates a certain numerical error. It is evident that halving the step size reduces the error to one-eighth ($\frac{1}{8} = (\frac{1}{2})^3$), showing that the truncation error is of order $\mathcal{O}(\Delta t^3)$, as expected when using a numerical scheme that is 2^{nd} order accurate.

Governing Equation of the Pad

The third test is aimed at verifying the correct solution of the pad's governing equation. This was carried out by comparing the pad response to the analytical solution of the mass–spring–damper system, given a set of parameters and initial conditions. The blocks were held stationary in their zero position in order to give the non-pad end of the pulling springs a fixed location.

Then, the pad was released with a known initial displacement and velocity.

The analytical solution is given by looking at the characteristic equation derived from the pad's governing equation:

$$m_x\lambda^2 + c_p\lambda + K = 0 \quad , \tag{3.11}$$

where $K = k_{p0} + Nk_p$ as in Section 3.1. For an underdamped system, the roots of the equation are complex, given by

$$\lambda_\pm = -\frac{c}{2m_x} \pm i\frac{\sqrt{4m_xK - c_p^2}}{2m_x} \quad , \tag{3.12}$$

whose real part yields the decay; and the imaginary part yields the damped frequency, of which we use the one with a positive sign. The pad response is thus described by

$$x(t) = e^{\mathrm{Re}(\lambda_+)t}\left[C_1\cos(\mathrm{Im}(\lambda_+)\,t) + C_2\sin(\mathrm{Im}(\lambda_+)\,t)\right] \quad , \tag{3.13}$$

with C_1 and C_2 depending on the initial displacement and velocity.

Given $m_x = 100, K = 200, c_p = 20, x(0) = 0.5, \dot{x}(0) = 0$, the pad position as a function of time is given by

$$x(t) = e^{-0.1t}\left[\frac{1}{2}\cos\left(\frac{\sqrt{199}}{10}t\right) + \frac{1}{2\sqrt{199}}\sin\left(\frac{\sqrt{199}}{10}t\right)\right] \quad , \tag{3.14}$$

and this function is drawn against an axis offset by -0.5 relative to that of the computed response in Figure 3.5.

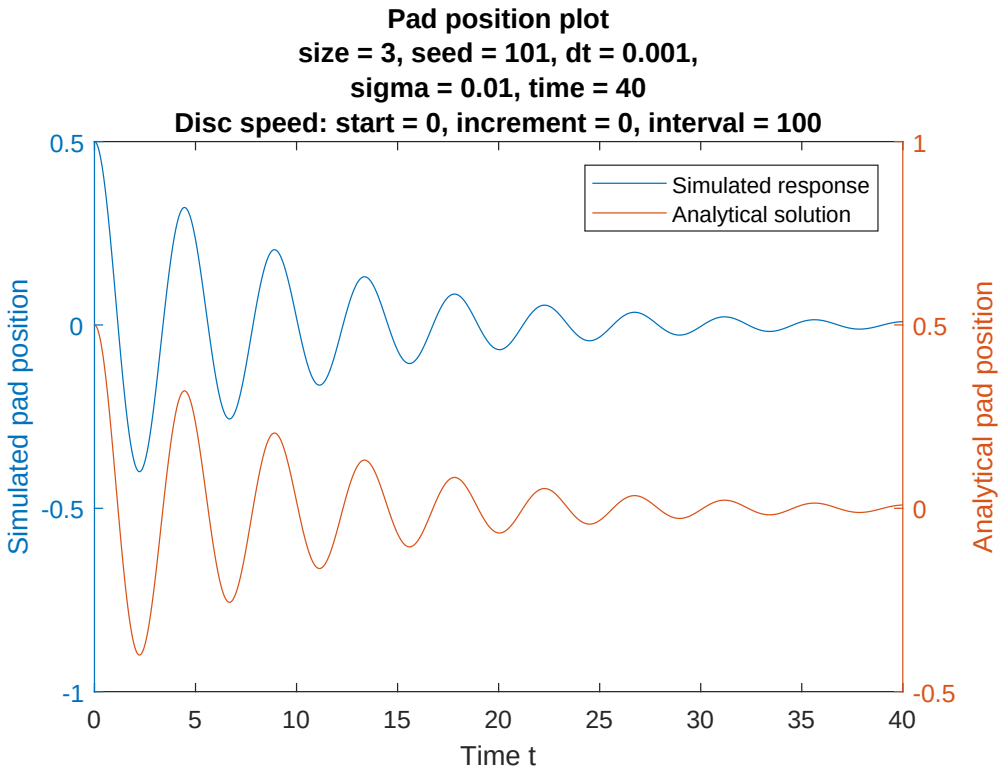

Figure 3.5: Computed pad response given known initial conditions (left-hand side y axis), compared to the analytical solution in Equation 3.14 (right-hand side y axis, note the -0.5 vertical offset).

3.4 Mechanism and Method

Mechanism

The program gives each block a random displacement $|u_j| \leq 0.75$, and as the disc moves at a speed of choice, the friction forces occurring in between will pull the blocks in the direction of the disc. Through the pulling springs, each block will interact with the pad, as well as with the adjacent block(s) through the neighboring spring(s). The pad's initial displacement and velocity are both zero, as the pad should be resting in zero position up until the point at which the brakes are applied.

Since the blocks are initially given a displacement not equal to the steady state position governed by the friction force and spring constants of the model, the blocks are expected to experience a "jump" which should introduce oscillations to the bodies in the model.

Results Processing Method

The program is set to run for a set amount of time units. For each time step, it will record the pad position, pad velocity, and the sum of forces on the pad from all the blocks. In addition, the positions of each block can also be recorded if needed; however, this leads to an undesirably large increase in computation time. Since the blocks are only a way of discretizing the outermost part of the brake pad surface, the significant output is limited to the sum of forces on the pad, which is hereinafter referred to as the *pad friction*.

The position, velocity, or friction on the pad can then be subjected to a spectrum analysis to investigate what frequencies make up the observed oscillations in the pad, for a given disc speed. Additionally, the disc speed can be set to increment by a certain value at any chosen time interval. This can be used not just to emulate the decreasing velocity as a direct result of braking, but also for obtaining results for multiple disc speeds all in one run. From there, one can plot the mean value and amplitude of the friction as a function of disc speed, optionally leaving out any transient features due to the sudden jolt from the momentary increase of disc speed.

In addition, simulations can be run as the Burridge-Knopoff model (Figure 2.1) or as a one degree-of-freedom model (Figure 2.3). This will be used to compare the behavior of the Burridge-

Knopoff–pad model with previously studied models.

3.5 Simulating Earthquake Events

The program has also been used to simulate earthquake events, based on the original Burridge-Knopoff model. In that case, the pad must be held stationary and act as the upper surface, since the only relevant governing equation is that of the blocks. Starting the blocks at a random displacement, they were pulled back by the substrate. When the force on at least one block exceeds the maximum static friction force, the relevant blocks will slip and gain a velocity from the pulling spring. The positions of all blocks are recorded, and the substrate is stopped. The blocks are then allowed to interact with each other until the movement dies out and the blocks have re-stuck to the slider, at which point the block positions are recorded again. This constitutes a slipping event. The substrate is then re-started again, and the process is repeated.

Retrieving the magnitude μ defined as the logarithm of the moment given by Equation 2.6, the events are sorted into a histogram-like plot, showing the frequency (i.e., amount of events for any given time span) as a function of magnitude. The results showed a scaling region, as indicated in Figure 3.6—similar to results by Carlson et al. (1991).

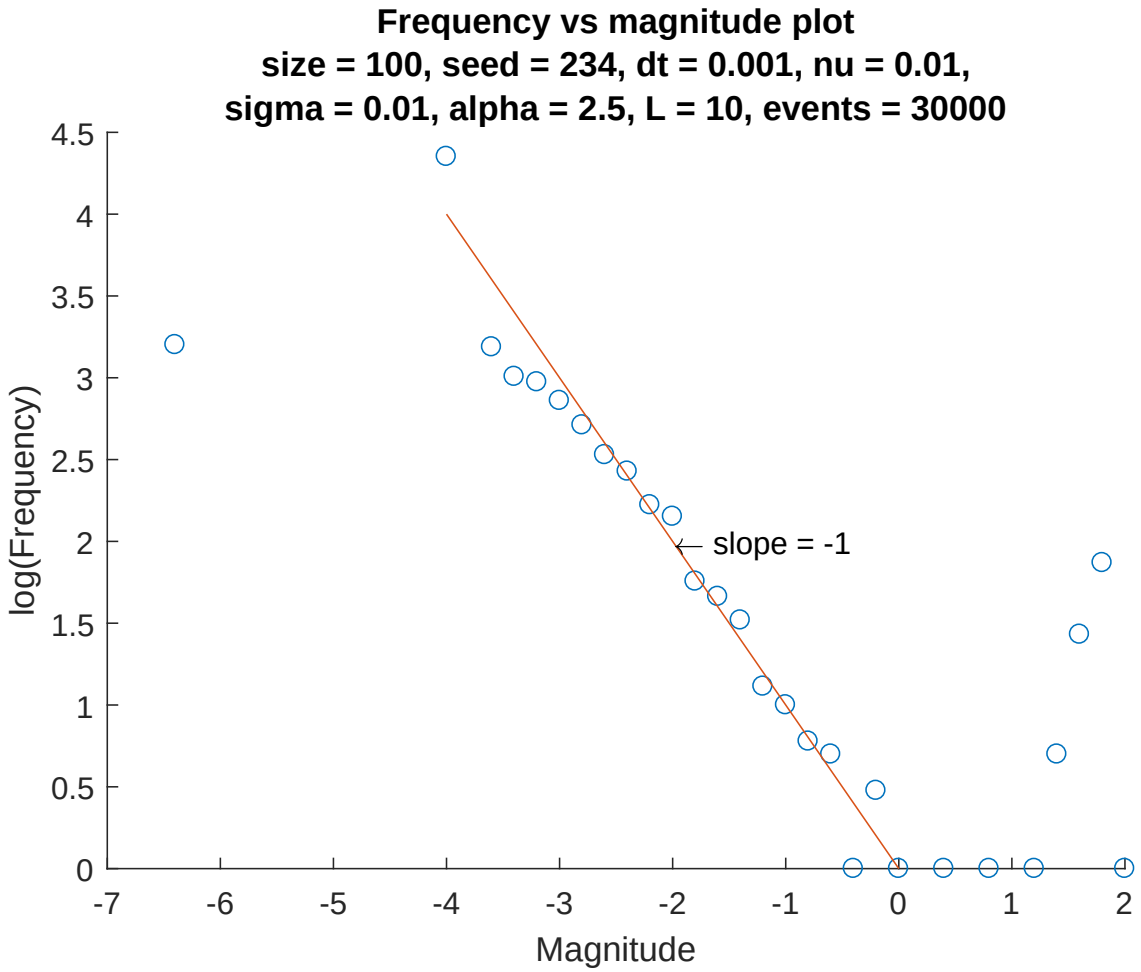

Figure 3.6: Magnitude distribution $D(\mu)$ for 30,000 events, showing the occurrence of a power law scaling region (see Equation 2.10). The magnitude bin size is 0.2.

Chapter 4

Results

In this Chapter, I will show results obtained from numerical simulations of the combined Burridge-Knopoff–Pad model. I will demonstrate and discuss pad movement at relevant speeds, perform a mean value–amplitude analysis, and identify areas of interest that needs further investigation. These areas will then be looked into with post-processing tools such as Fourier spectrum analyses. Where necessary, results will be compared to existing models, namely the plain Burridge-Knopoff Model and the one degree-of-freedom model.

4.1 Pad Movement

The pad moves as a consequence of the pulling springs that make the pad follow the movement of the blocks as the disc pulls them backwards. On the other side of the pad, visually speaking, the spring and damper that connect it with the stationary caliper will exert forces on the pad in the opposite direction as the pad follows the blocks. Simulations having several blocks start out with the blocks being randomly displaced in the range -0.75 to 0.75, as also stated in Section 3.4. The pad starts out in its zero position.

As a general rule, the initial disc speed, its increment, and the interval at which the speed is incremented are always indicated in the text above each graph. A part of the signal corresponding to one disc speed constitutes what will be referred to as a *speed segment*. Although we study the model behavior as a result of a given disc speed, the position, velocity, and friction are plotted in the time domain. This is due to the fact that any increment greater than Δt gives a speed

segment longer than a time step, resulting in a discrete disc speed axis. Plotting a continuous graph on a discrete axis would be misleading and inaccurate.

The pad does not experience friction itself; in these plots, the friction is the sum of the forces from all blocks. However, since the blocks are just a way of approximating the pad surface which is in contact with the rotating disc, it represents the friction experienced by the pad.

Stick–Slip Behavior

Figure 4.1 shows the pad as the simulation is started with disc speed $v = 0.005$. The speed is increased by 0.005 every 2000^{th} time unit. The small oscillations from $t = 0$ are due to the pad being released, moving to reach equilibrium given the friction and non-zero block positions. As these oscillations are damped out, there is a region where the pad is being pulled backwards by the blocks until one or more of them slip. The pad can then be seen quickly snapping back.

Figure 4.2 shows the pad velocity for the same time span. Each slipping event shows up as a high-amplitude peak resembling electrocardiogram "blips." The disc speed increase at $t = 2000$ is reflected by the pad velocity in the stick phase, as well as the smaller period between slips. It is, however, noticeable that the stick phase is not, with the exception of the first one, a straight line; rather, it slowly builds up with very small oscillations. In addition, the peaks are of irregular amplitude and spacing with respect to time.

The cause of these irregularities is the fact that the blocks are randomly displaced. If the blocks were equally spaced, they would all be subject to the exact same forces at any given point in time and thus behave as though they were one single block. There would therefore be no irregularity as this is caused by the relative displacement of two or more blocks. The single big peak indicates a slipping event involving all the blocks, thereby allowing the pad to snap back a great distance, while the small "build-ups" before the major slip only involve a smaller amount of blocks. Carlson and Langer (1989) noted that in the plain Burridge-Knopoff model, irregularities were amplified during a slipping event. This could explain why each stick-phase is increasingly irregular. This increase in irregularity is most visible between $t = 0$ and $t = 2000$, i.e., where there has been no disc speed increase. This is because a disc speed increase is executed rather abruptly, which kicks the system through the sudden change in friction. This kick may then result in some sort of pulse at the start of each speed segment.

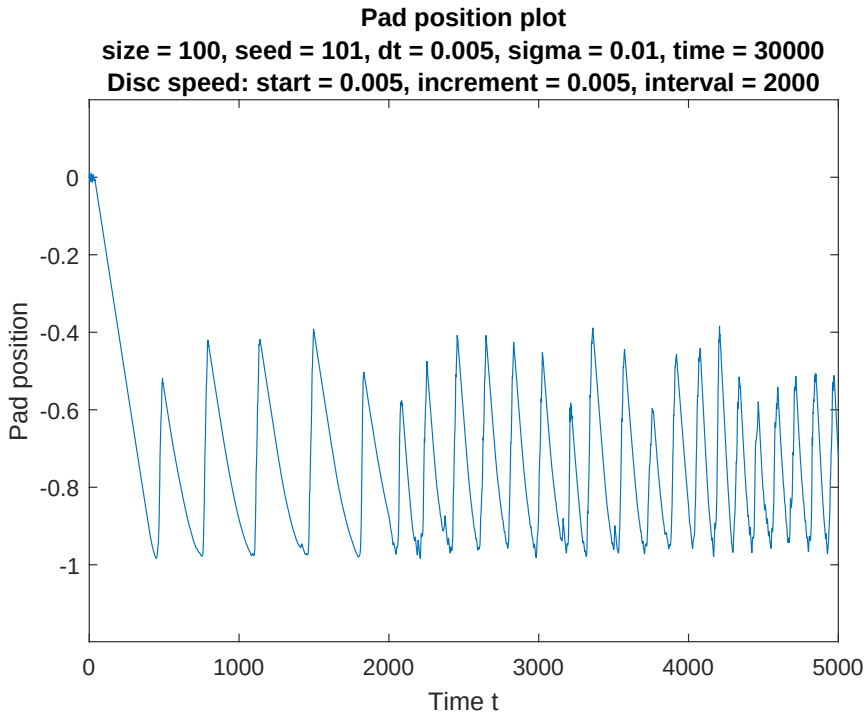

Figure 4.1: Pad position plot showing stick–slip behavior. The blocks are sticking, not the pad, but the latter's position follows that of the former. $v = 0.005, 0.01, 0.015$

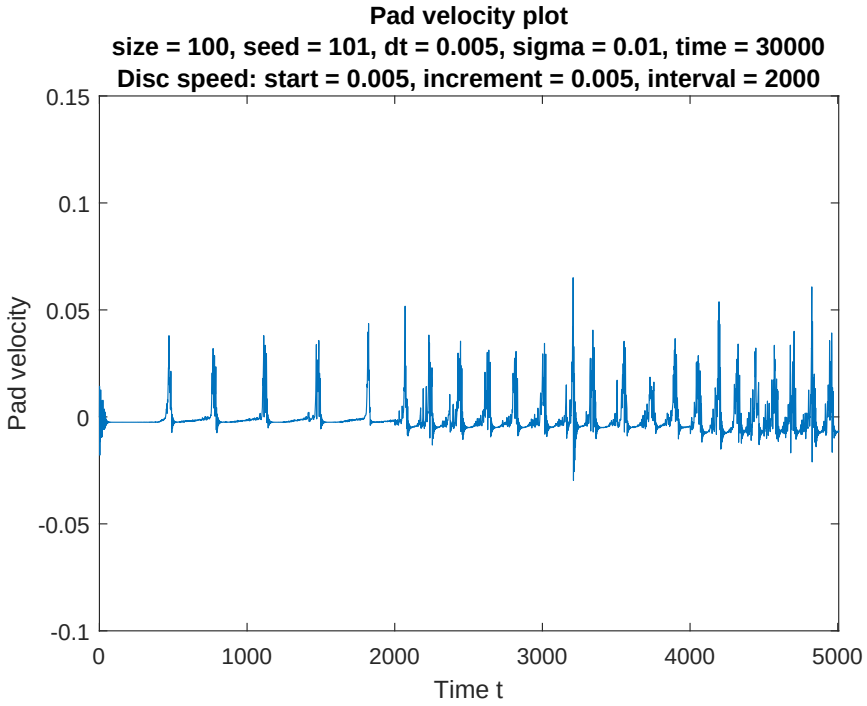

Figure 4.2: Pad velocity plot. Slipping events show up in a form similar to ECG "blips," where the pad exhibits a high velocity in the opposite direction until the blocks again stick, and the pad oscillations are damped out. Note how, as the disc speed increases (backwards), the flat stick phase velocity follows.

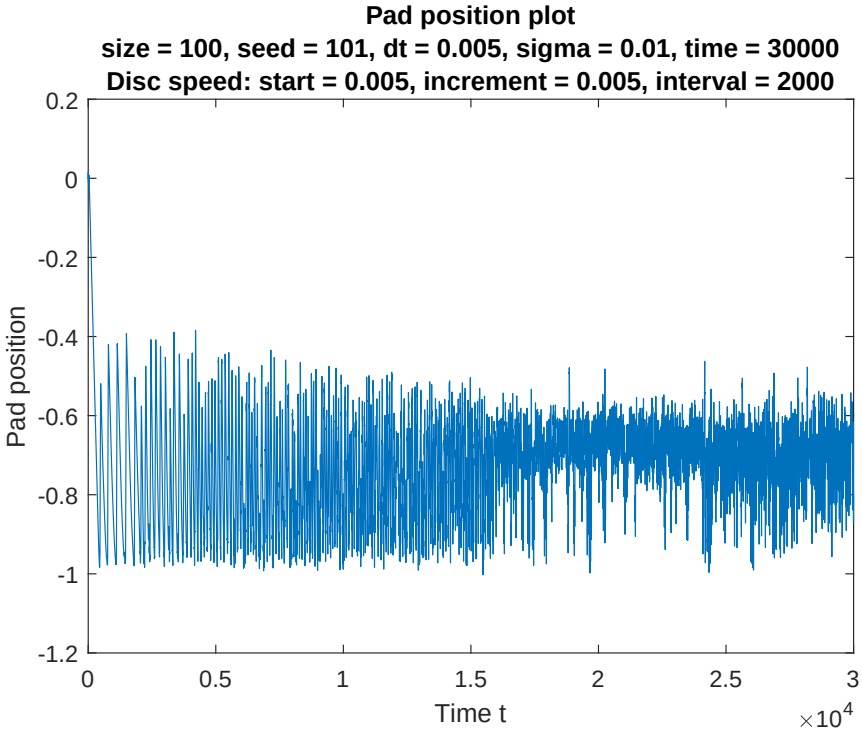

Figure 4.3: Pad response for $v \in [0.005, 0.075]$.

Varying Amplitudes

For different disc speeds, the pad shows oscillations in position, velocity, and friction of varying amplitudes. The amplitudes do not necessarily need to be regular and scaling with the disc speed. An example of this is shown in Figure 4.3. For instance, note the region between $t = 16000$ ($v = 0.045$) and $t = 24000$ ($v = 0.065$), which, in addition to some larger peaks, has a generally smaller amplitude and a mean value closer to zero. Figures 4.4 (a) and (b) show a smaller sample outside and inside of this region, respectively.

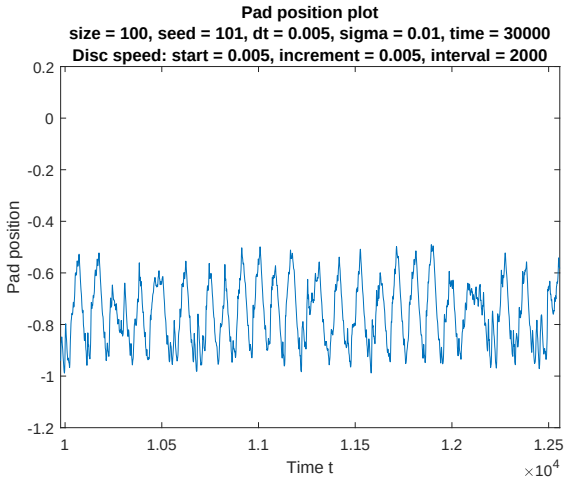

(a) $v = 0.003$ for $t \in [10000, 12000)$.

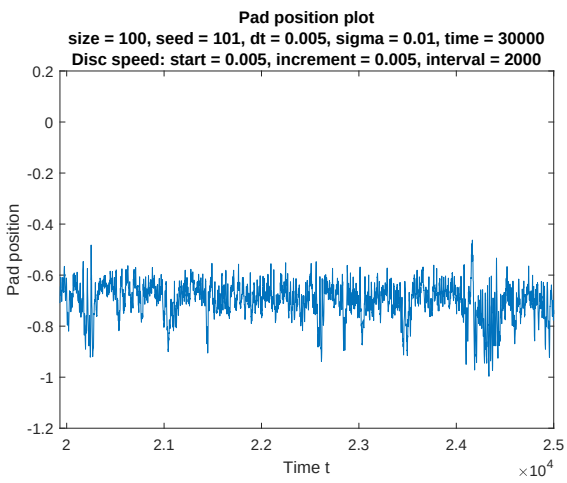

(b) $v = 0.055$ for $t \in [20000, 22000)$, $v = 0.06$ for $t \in [22000, 24000)$.

Figure 4.4: Two closeups of the pad position at different times, showing the pad response at the corresponding disc speeds.

Continuous Increase and Decrease of the Disc Speed

Simulations were also run in which the disc speed was changed pseudo-continuously, specifically with an increment every time unit so that the speed went either from 0 to 1, or from 1 to 0, over 40,000 time units. The pad position for the simulation with disc speed decreasing at an interval of 1 time unit is shown in Figure **??**. The pad shows a period of large oscillations between speeds 0.91 and 0.88, in addition to shorter periods of similarly large oscillations. Later, as the speed is decreasing, the amplitude follows. Then, at the very end, when the disc speed is about 0.0375, the pad goes into stick–slip behavior until the disc has stopped completely.

As this model is still in its early stages of study, the situation where the disc speed is continuously changing is too complex to understand. Therefore, for the remainder of this Chapter, the analyses will be performed on the data obtained from simulations with long intervals of constant disc speed. However, this would be a good topic to study in the future.

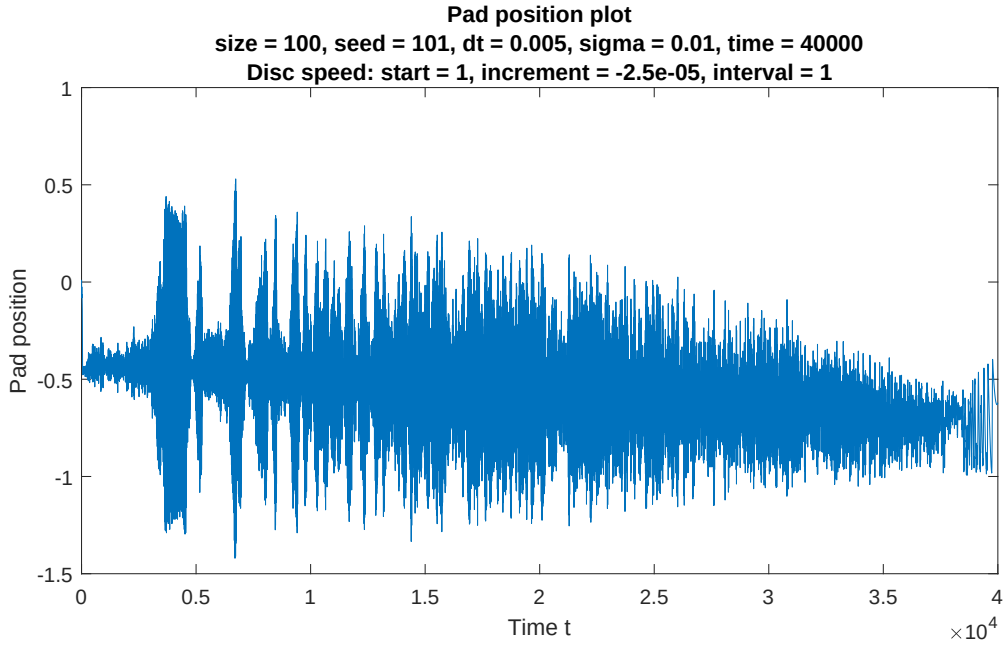

Figure 4.5: Pad position with a disc speed decreasing at an interval of 1, all the way down to 0.

4.2 Friction Study

In order to find out how the combined Burridge-Knopoff–Pad model differs from other models, the respective results must be compared. Figure 4.6 shows the amplitude and mean value of the friction on the pad as a function of disc speed. There are four pairs of lines corresponding to four different model configurations, which will be explained in the upcoming Subsection. Each line is assembled from five simulations with different disc speeds, and the boundaries between these are visible as gaps. Note that the disc speed axis is logarithmic, showing speeds from 0.005 to 1, so as to better show the low speeds which were taken from simulations with a smaller speed increment. Additionally, for comparison purposes, the pad position amplitude is included as a dashed light blue line, scaled by the pad mass in order to be of the same order as the friction. The solid dark blue line is the friction law (see Figure 3.2). Please note that the disc speed, as previously mentioned, is discrete, and so are the plotted values. However, I've chosen to connect these points with lines in order to make it easier to see how the values change given different disc speeds.

In order to provide an accurate reading, the results are obtained by taking only the last half of each speed segment, so as to leave out any transient effects resulting from the "kick" given to

the system by the disc speed increment. For the sake of explaining the processing of data, this second half of the speed segment is referred to as the *input signal*.

The mean value is found simply by taking the average of the input signal. It shall here be noted, as also indicated in the legend, that the mean values are plotted with the opposite sign so as to keep all lines above the disc speed axis. The amplitude is found by obtaining the root mean square error from the mean value, with a prefactor of $\sqrt{2}$ so as to give the actual amplitude. Furthermore, the amplitude and mean value lines include error bars, which show the error given by the standard deviation of the amplitude and mean values when taking a 4 block average on the input signal. Thus, shorter error bars signify a more uniform input signal, and therefore gives an indication of the reliability of that particular reading.

Error Calculation

Given a signal S with N points S_i, $i \in [1, N]$, its mean value is defined as

$$\bar{S} = \frac{1}{N} \sum_{i=1}^{N} S_i \quad , \tag{4.1}$$

and it's amplitude A_S is given by

$$A_S = \sqrt{2} \sqrt{\frac{1}{N} \sum_{i=1}^{N} (S_i - \bar{S})^2} \quad . \tag{4.2}$$

Block averaging can be done on either of these properties. In the case of Figure 4.6, it is done on both. Taking the block average of a signal property Y, we split the signal into M blocks and compute the property Y_j for each block j. The standard deviation σ is defined as the square root of the variance (normalized by M):

$$\sigma = \sqrt{\frac{1}{M} \sum_{j=1}^{M} (Y_j - \bar{Y})^2} \quad , \tag{4.3}$$

where the mean $\bar{Y}$ already is the global value of property Y.

The error ϵ is then given by

$$\epsilon = \frac{\sigma}{\sqrt{M}} \quad . \tag{4.4}$$

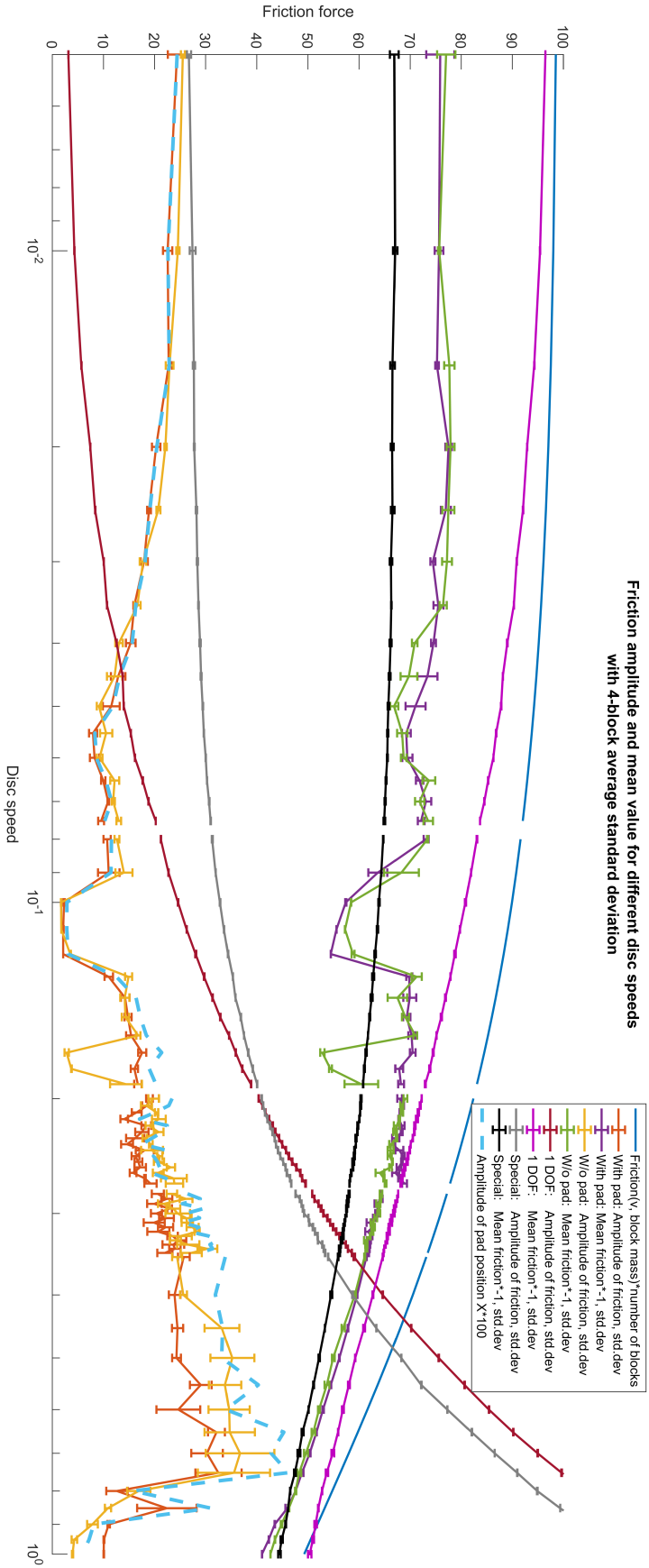

Figure 4.6: Friction amplitudes and mean value for different model configurations, and the friction law and pad position multiplied by the pad mass. Logarithmic horizontal axis. $v = 0.005$ to $v = 1$

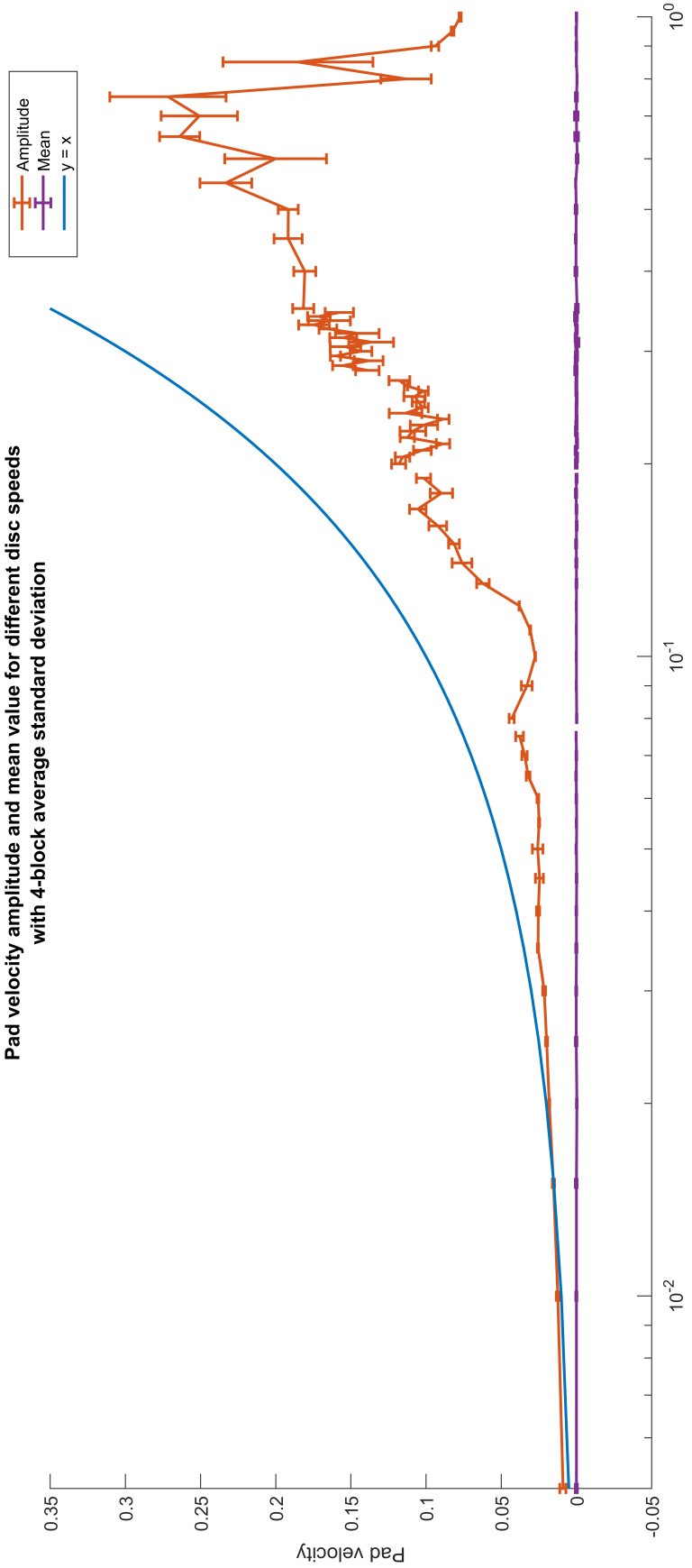

Figure 4.7: Burridge-Knopoff–Pad model only: Pad velocity amplitude. Logarithmic horizontal axis. In addition, the line $y = x$ has been added for easy comparison of the graph to a linear increase. $v = 0.005$ to $v = 1$

Model Configurations

Figure 4.6 shows a total of ten lines, of which the two in the dark and light shades of blue are the friction law and the amplitude of the pad position scaled by the pad mass, respectively. Three other pairs of lines correspond to three different model configurations:

- **Combined Burridge-Knopoff–Pad Model** (w/ pad);
- **Burridge-Knopoff Model** (w/o pad), the pad is held stationary, leaving the system equal to the original Burridge-Knopoff Model; and,
- **1 Degree-of-Freedom Model** (1DOF), using one block only and having the pad and block act as one.

Finally, he black and gray lines, denoted in the legend as *special*, show the friction amplitude and mean for a 1 DOF system where the friction law is set to equal the green line in the figure, i.e., the friction experienced by the stationary pad in the original Burridge-Knopoff model. However, since our simulations only include disc speeds between 0 and 1, and the relative velocity between disc and block is not bound by this range, this special friction law is continued by the original friction law, scaled down to fit the endpoint of the new part. Furthermore, the special friction is mirrored such that it is an odd function. The special friction law with its continuation indicated as a red line is shown in Figure 4.8.

The special 1 DOF simulation was included in order to subject the 1 DOF model with the same friction experienced by the plain Burridge-Knopoff model. Thus, we can compare this response with the Burridge-Knopoff–Pad model.

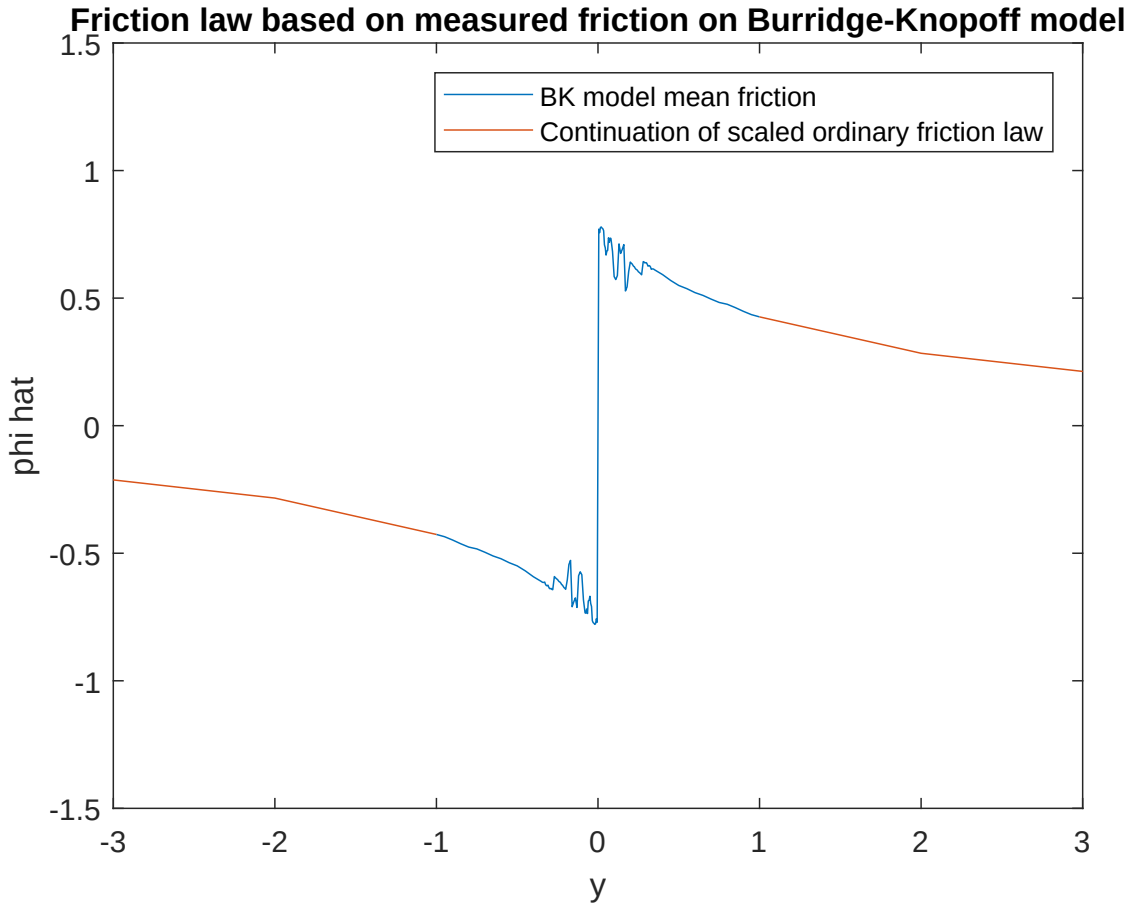

Figure 4.8: Special friction law with continuation of original friction for input $|y| > 1$.

4.3 Investigation of Areas of Interest

In this Section, I will identify and investigate areas of interest stemming from the friction amplitude–mean value plot (Figure 4.6).

Oscillation Drop

Looking at the Burridge-Knopoff–Pad and plain Burridge-Knopoff lines at small disc speeds, they exhibit one and two oscillation drops, respectively. The relevant portion in the friction and velocity amplitude–mean plots is shown in Figure 4.9 (a) and (b), respectively; and the corresponding pad friction plots are shown in in Figure 4.10. Naturally, the velocity plot in Figure **??** naturally only applies to the Burridge-Knopoff–Pad model—the only model in which there is a pad.

In order to investigate what happens between the 0.08, 0.09, 0.1, and 0.11 segments, we look at the block trajectory. I've chosen to look at three adjacent non-edge blocks. Figure 4.11 shows three block positions superimposed over that of the pad, showing the transition between a chaotic high-amplitude portion and the low-amplitude "drop" portion, while Figure 4.12 (a) and (b) give a closer look at two different disc speeds on each side of the transition.

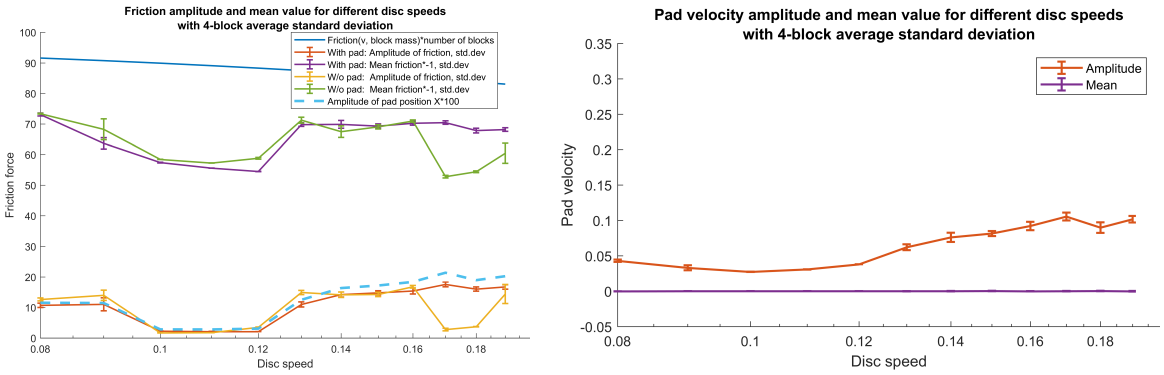

(a) Friction (b) Velocity (BKP only)

Figure 4.9: Amplitude–mean plots over a portion containing oscillation drops.

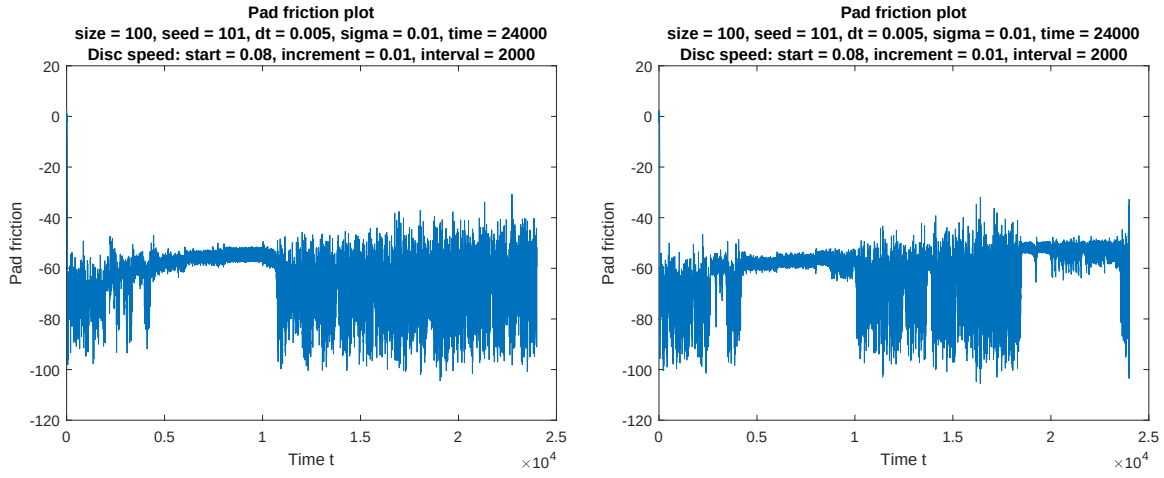

(a) Burridge-Knopoff–Pad (b) Plain Burridge-Knopoff

Figure 4.10: Friction in the Burridge-Knopoff–Pad and the plain Burridge-Knopoff models. v from 0.08 to 0.19.

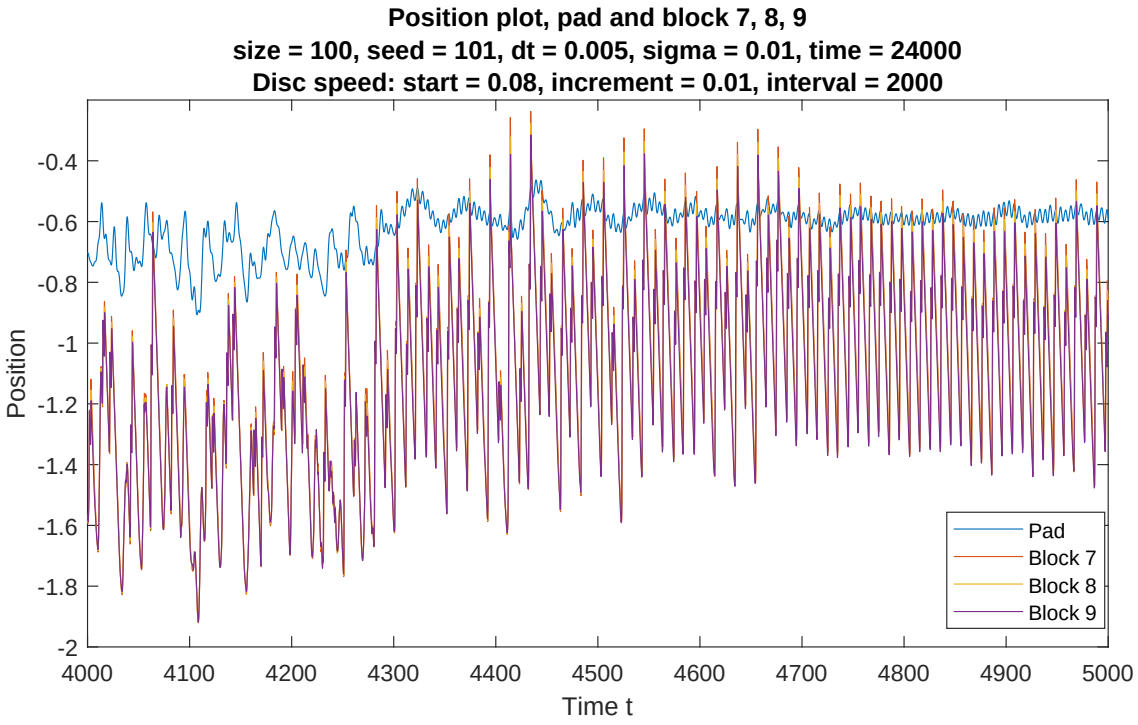

Figure 4.11: Three block and pad positions, showing a transition into a region with even oscillations. $v = 0.1$

As is clearly visible in Figure 4.11, the vibration of the pad and blocks undergo a transition into an even pad oscillation with a low amplitude. The plot starts at $t = 4000$, which is the point where the disc speed is set to 0.1. What follows is most likely a transient feature due to the speed increment "kick," and the system eventually stabilizes from noisy behavior into even motion.

The noisy behavior can be explained by the fact that the blocks still are in the stick–slip region. Figure 4.12 show three block positions as well as the pad position for disc speeds v equal to 0.09 and 0.12. The pad oscillation can easily be described as noisy. Note that the blocks' stick–slip motion is uneven. For example, in (a), at $t = 3110$, the blocks are pulled back until they slip, then they travel forward but re-stick, likely due to the behavior of adjacent blocks not included in the figure. As the blocks have re-stuck, they are again pulled backwards until the point where they slip—along with the rest of the blocks, judging by the magnitude. Such small slipping events will naturally affect the pad.

Looking at Figure 4.12 (b), where the disc speed is increased to $v = 0.12$, the oscillations become periodic. A higher disc speed will decrease the friction of the blocks, thereby reducing the risk of minor slipping events that are the case for $v = 0.09$.

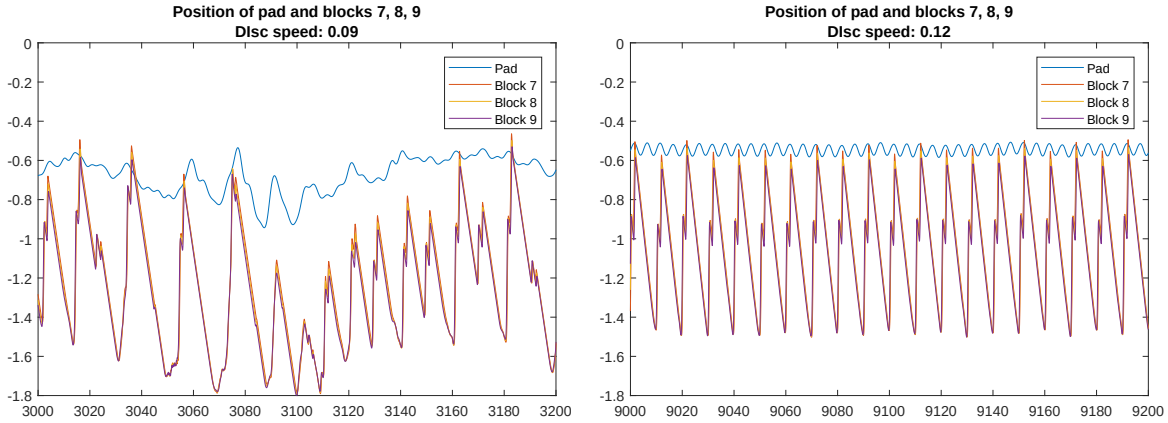

(a) $v = 0.09$ (b) $v = 0.12$

Figure 4.12: Position of the pad and three blocks, for two different disc speeds.

Figure 4.13 (a) and (b) show the Fourier spectrum analyses of the position of the pad and block 7. What's interesting to note here is the pad wave component of frequency 0.2. The pad's natural frequency is given by (see Table 3.1 for parameter values):

$$f_n = \frac{1}{2\pi}\omega_n = \frac{1}{2\pi}\sqrt{\frac{k_{p0} + Nk_p}{m_x}} \approx 0.2256 \quad . \tag{4.5}$$

The damped frequency is then given by

$$f_d = f_n\sqrt{1-\zeta^2} \approx 0.2249 \quad . \tag{4.6}$$

The even oscillations are thus approaching the pad's natural frequency, albeit not reaching it completely. This could be due to the one small stick phase within each slip phase, clearly visible in Figure 4.12, which can help slow down the pad, ever so slightly. The pad movement will of course also make a contribution to this smaller stick incident. However, considering that the pad motion is governed by how the blocks move, there may not be a reason for the pad to oscillate in its natural frequency. While the stick–slip motion may well be periodic, its period does not have to correspond to that of the pad.

A block's natural frequency is similarly given as

$$f_n = \frac{1}{2\pi}\omega_n = \frac{1}{2\pi}\sqrt{\frac{k_p + 2k_c}{m_u}} \approx 2.256 \quad , \tag{4.7}$$

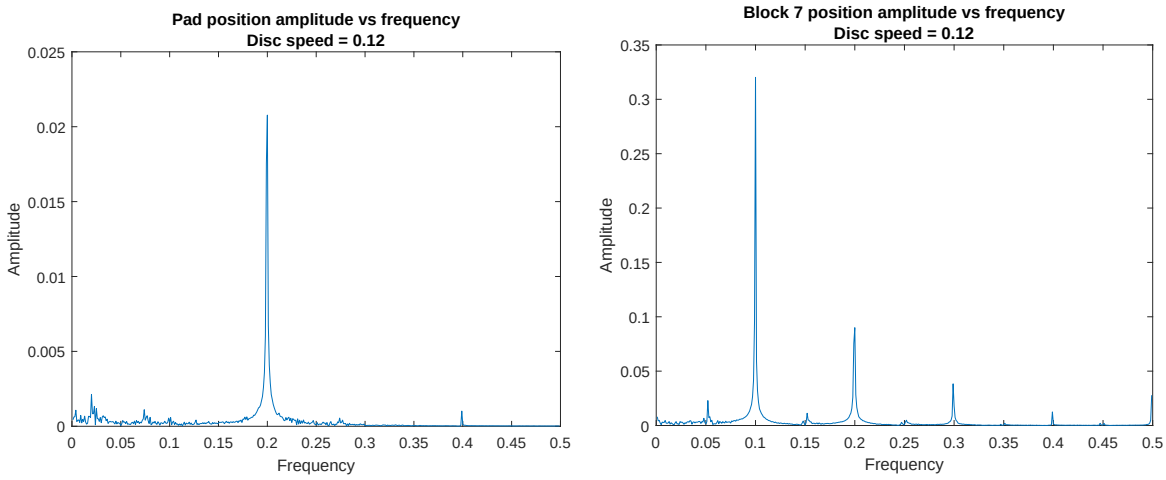

(a) Pad (b) Block 7

Figure 4.13: Fourier spectrum analyses of the pad (a) and block 7 (b) positions. v = 0.12

a frequency which is not observed in the even region. However, since the friction acts as a damper, the actual frequency could be lower. This would anyway not be present in any stick–slip region.

Plain Burridge-Knopoff Oscillation Drop

The oscillation drop unique to the plain Burridge-Knopoff model as shown in Figure 4.10 (b) occurs between disc speeds $v = 0.16$ and 0.17.

The Fourier spectrum analysis of the "pad" friction in the plain Burridge-Knopoff model is shown in Figure 4.14. Disregarding the peak close to zero frequency (zero frequency itself has been removed), the frequency with the biggest amplitude is 0.3. However, we see other harmonics of 0.15 in the plot. This is also far away from the block natural frequency.

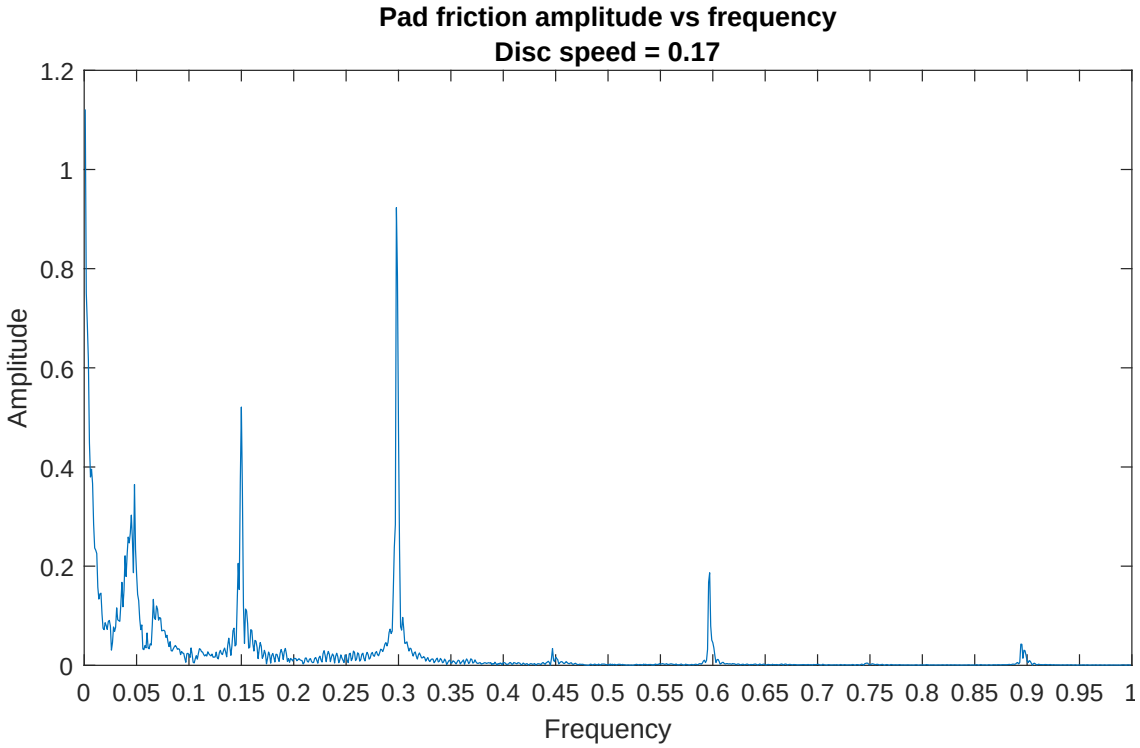

Figure 4.14: Fourier spectrum analysis of pad friction in the plain Burridge-Knopoff model, $v = 0.17$

Special Speed

In the early phases of testing the simulation, a "special speed" was derived. A system of equally spaced springs (equal to a system of one spring, given the proportionality of the parameters) was pulled backwards until it slipped. Then, time was recorded as the block was allowed to oscillate until the friction had dissipated all energy. This time t_{death} is then used along with the maximum static friction force, and the spring constant, thus:

$$v_{\text{special}} = \frac{F_0}{k_p}\frac{1}{t_{\text{death}}} \quad . \tag{4.8}$$

$t_{\text{death}} = 3.589$ gives $v_{\text{special}} \approx 0.28$.

Figure 4.15 shows a portion of Figure 4.6 around the special speed. In the vicinity of the speed, we can note several observations.

The plain Burridge-Knopoff simulation exhibits the previously explained oscillation drop. Later, along the speed axis, the BK oscillations have recovered, and its amplitude is showing tendencies to be departing from the BK–Pad friction amplitude, but at the same time, the BK–Pad mean friction departs from that of the BK simulation. Finally, a section where the (scaled) pad position amplitude becomes greater than the BK and BKP friction amplitudes.

At this point, we do not know whether these observations are related to this special speed, and so this is a good example of something in need of further study.

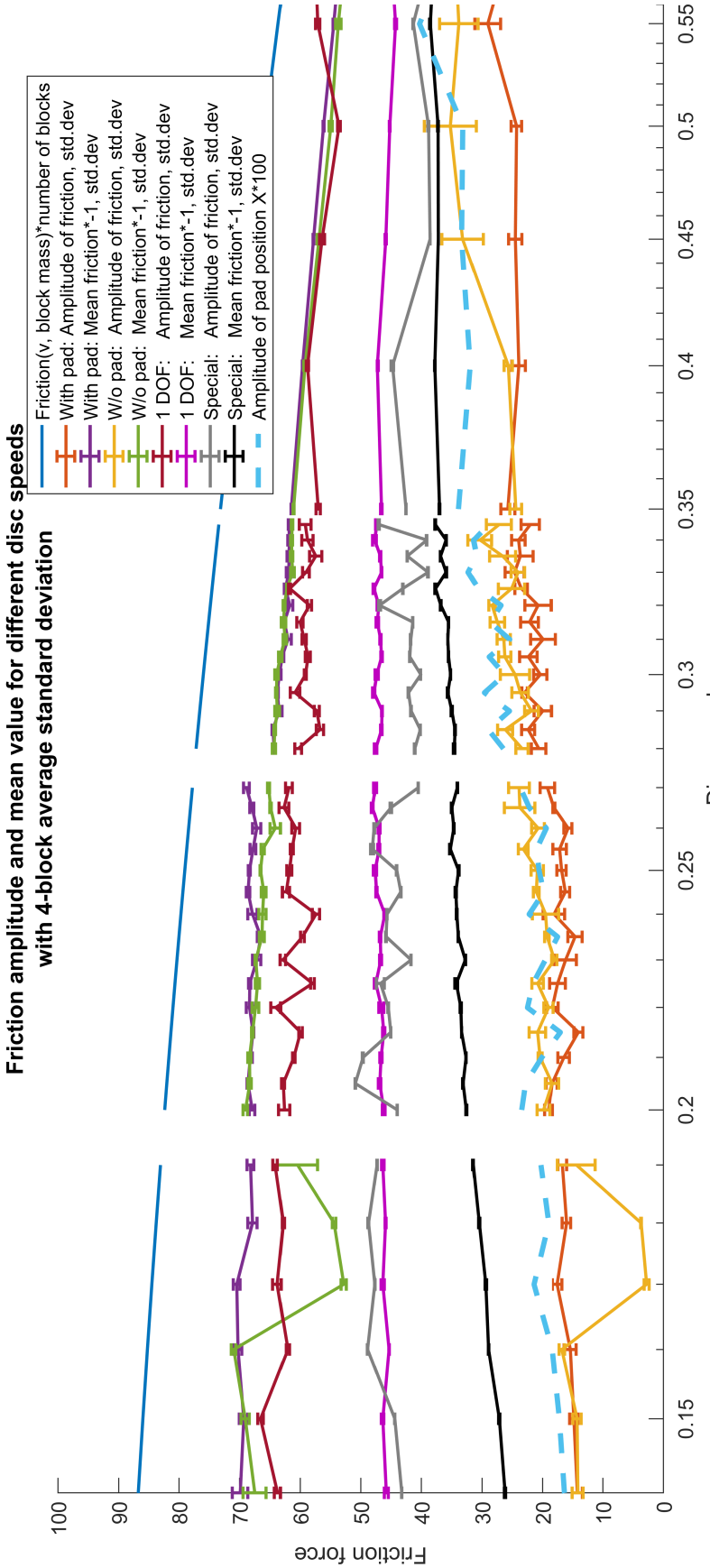

Figure 4.15: Friction amplitude and mean values for disc speeds around the special speed. The gap indicates between two parts of the simulation; the plot is anyway, as previously mentioned, not continuous.

4.4 Model Differences

Judging by Figure 4.6, there are differences between the behavior of the Burridge-Knopoff–Pad and the plain Burridge-Knopoff models. However, for greater disc speeds, the friction amplitude and mean values generally follow the same development. On the other hand, the difference between the mentioned models and the two one degree-of-freedom simulations is vast.

The most noticeable difference between the Burridge-Knopoff–Pad and plain Burridge-Knopoff models is the second drop in friction exhibited by the plain BK model, in the disc speed range $v = 0.17$ through 0.19. However, the Fourier analysis did not provide any hints as to why this is the case, and so the real cause of this drop is not clear at this point. Perhaps, what's most important is to find out why the Burridge-Knopoff–Pad model *doesn't* show the same drop. Another difference can be seen around $v = 0.5$, where the mean friction value of the plain Burridge-Knopoff model shows an increase. The time-domain result is relatively chaotic, resulting in the bigger error bars that are clearly visible in Figure 4.6.

The one degree-of-freedom model showed amplitudes that were strictly increasing, at least for the range studied in this Thesis. There could be a drop at even higher speeds, similar to what the BKP and BK models show at disc speed $v = 0.9$. The question is whether to use this 1 DOF model in further study of brake squeal. The answer is most likely no, as has also been concluded in literature. What is interesting, though, is the fact that at disc speed $v = 0.2$, the 1 DOF model with the normal friction law surpasses the special friction 1 DOF model with respect to amplitudes. Nevertheless, it did not provide results near the BKP model.

Chapter 5

Summary and Recommendations for Further Work

5.1 Summary and Conclusions

In this Thesis, I have presented a new model, which, to the best of my knowledge, has never been studied before. Along with an account of the background, including an overview of relevant models and literature on brake squeal, as well as the application of the Burridge-Knopoff model to the study of earthquakes, the new Burridge-Knopoff–Pad model was developed, implemented, and simulated.

The model is not necessarily complete. However, it represents the first step toward a model where the previously studied small-scale friction dynamics are combined with an unstable resonator. As a result, we have a model which can be used to describe the interaction between these two aspects, and its application is not limited to brake systems. Rather, other systems that need to consider the interaction between friction and structural resonance, such as kinetic art, could make use of this model. Although only a model that will never be a hundred percent realistic, I think the enhancement of the Burridge-Knopoff model, in which we allow a larger mass in the model to oscillate, is a step in the right direction regarding realisticness, although further study is needed.

The Burridge-Knopoff–Pad model shows a couple of interesting characteristics that either differ from, or are unable to occur in, the plain Burridge-Knopoff model. The most obvious

example is of course how the pad itself is allowed to move, thereby having its own properties such as a natural frequency. Furthermore, the addition of the pad introduces a new degree-of-freedom, giving rise to new vibration modes.

By and large, I have based my results on parts of the response simulated with segments of constant disc speed. This was due to the fact that the model is new and unstudied, and in order to understand the basic behavior, the simulations must be kept basic. Hence the idealized friction law, equal masses and springs, and so on.

5.2 Discussion

The Burridge-Knopoff–Pad model has in many ways provided insight into situations where structural oscillation is combined with friction. Differences in pad friction, both in mean value and amplitude, can be seen, with an acceptable error. The error may be reduced by using a longer disc speed interval, but it shall also be noted that the error will be greater, the noisier the signal.

The one degree-of-freedom model is probably not suitable, as has been stated by several papers. However, it's a hard model to compare to the multi-degree-of-freedom models, as there is only a block, making it hard to define which part of the brake assembly it represents. Additionally, if one generally needs to take the entire brake assembly into consideration if one is to perform a realistic simulation, maybe the Burridge-Knopoff–Pad is insufficient, too. However, the BKP model might provide new insight, although it will need further study under different conditions and parameters.

5.3 Recommendations for Further Work

As this model is new and unstudied, this introductory study leaves many areas which can be recommended for future study. The model was kept completely basic in order to understand the basic characteristics and behavior. Therefore, later studies should aim to eliminate such simplifications; however, in a slow and careful manner, so as to not miss out on anything.

One of the first things to be done is to allow the continuous change of disc speed in the simulation. It is not a given fact that the model will behave the same. Furthermore, Figure 4.5

showed an interesting region indicated in the text, which should be investigated.

The introduction of the pad adds another degree of freedom to the system. Therefore, one should perform analyses of the different modes of vibration in the system, preferably also investigate what parameter values are needed in order to trigger the different modes of vibration.

Further into the future, steps should be taken to implement a more realistic friction law. Empirical data for the friction would naturally be the most realistic option, however the model itself is only an approximation, so this might not be of great importance unless the model is further expanded to reflect a realistic brake assembly. Use of variable friction based on random figures could be sufficient, and it could be interesting to see how this affects the oscillation properties.

Bibliography

Brockley, C. A., Cameron, R., and Potter, A. F. (1967). Friction-induced vibration. *Journal of Lubrication Technology*, 89(2):101.

Burridge, R. and Knopoff, L. (1967). Model and theoretical seismicity. *Bulletin of the Seismological Society of America*, 57(3):341–371.

Cantoni, C., Cesarini, R., Mastinu, G., Rocca, G., and Sicigliano, R. (2009). Brake comfort - a review. *Vehicle System Dynamics*, 47(8):901–947.

Carlson, J. M. and Langer, J. S. (1989). Mechanical model of an earthquake fault. *Physical Review A*, 40(11).

Carlson, J. M., Langer, J. S., Shaw, B. E., and Tang, C. (1991). Intrisic properties of a burridge-knopoff model of an earthquake fault. *Physical Review A*, 44(2).

Coudeyras, N., Nacivet, S., and Sinou, J.-J. (2009). Periodic and quasi-periodic solutions for multi-instabilities involved in brake squeal. *Journal of Sound and Vibration*, 328(4-5):520–540.

Denimal, E., Nacivet, S., Nechak, L., and Sinou, J.-J. (2017). On the influence of multiple contact conditions on brake squeal. *Procedia Engineering*, 199:3260–3265.

Galvanetto, U. (1999). Non-linear dynamics of multiple friction oscillators. *Computer Methods in Applied Mechanics and Engineering*, 178(3-4):291–306.

Hoffmann, N., Fischer, M., Allgaier, R., and Gaul, L. (2002). A minimal model for studying properties of the mode-coupling type instability in friction induced oscillations. *Mechanics Research Communications*, 29(4):197–205.

Ibrahim, R. A. (1994). Friction-induced vibration, chatter, squeal, and chaos—part II: Dynamics and modeling. *Applied Mechanics Reviews*, 47(7):227.

Kinkaid, N., O'Reilly, O., and Papadopoulos, P. (2003). Automotive disc brake squeal. *Journal of Sound and Vibration*, 267(1):105–166.

Matsui, H., Murakami, H., Nakanishi, H., and Tsuda, Y. (1992). Analysis of disc brake squeal. In *SAE Technical Paper Series*, number 920553. SAE International.

Ostermeyer, G. P. (2010). On tangential friction induced vibrations in brake systems. In Thomsen, P. and True, H., editors, *Non-smooth Problems in Vehicle System Dynamics*. Springer-Verlag Berlin Heidelberg.

Ouyang, H., Nack, W., Yuan, Y., and Chen, F. (2005). Numerical analysis of automitice disc brake squeal: a review. *Int. J. Vehicle Noise and Vibration*, 1(3/4):207–231.

Rhee, S., Tsang, P., and Wang, Y. (1989). Friction-induced noise and vibration of disc brakes. *Wear*, 133(1):39–45.

Spurr, R. T. (1961). A theory of brake squeal. *Proceedings of the Institution of Mechanical Engineers: Automobile Division*, 15(1):33–52.

Xia, J., Gould, H., Klein, W., and Rundle, J. B. (2005). Simulation of the burridge-knopoff model of earthquakes with variable range stress transfer. *Physical Review Letters*, 95(248501).